Fakultät für Physik und Astronomie
Ruprecht-Karls-Universität Heidelberg

Bachelorarbeit
im Studiengang Physik
eingereicht von

Stefan Grohnert

geboren in Detmold

2016

Development of an Exposure Time Calculator for CARMENES

Die Bachelorarbeit wurde angefertigt von Stefan Grohnert an der
Landessternwarte Königsstuhl der Universität Heidelberg
unter der Betreuung von
Dr. Sabine Reffert

Zusammenfassung

CARMENES beobachtet M-Zwerge auf der Suche nach Exoplaneten. Ein halbes Jahr mit Beobachtungen am Calar Alto sind nun vergangen und die Erfahrungen aus dieser Zeit sollen in die kommenden Beobachtungen positiv mit einfließen. Bis jetzt beruhten alle Belichtungszeiten auf einer Zeitentabelle und der Erfahrung der Beobachter um die Beobachtungsbedingungen auszugleichen.
Diese Arbeit analysiert nun alle gemachten Beobachtungen des Projekts, um einen Belichtungszeitrechner (ETC) zu erstellen und damit die Qualität und das Zeitmanagement der kommenden Beobachtungen zu verbessern. Eine minimale Beobachtungszeit, basierend auf den Eigenschaften des Sterns, muss bestimmt werden und desweiteren wird untersucht, welche Anpassungen aufgrund der Beobachtungsbedingungen angebracht werden müssen.
Das Ergebnis der Arbeit bietet den Beobachtern dann eine neue Orientierung, um eine brauchbare Beobachtungszeit auszuwählen oder zu prüfen ob andere Projekte mit der Konfiguration des Spectrografen brauchbare Ergebnisse erhalten.

Abstract

CARMENES observes M dwarfs to search for Exoplanets. Now half a year of observations are done at Calar Alto and the practical experience of this time should influence future observations positively. Until now the exposure times were based on a time table and the observer experience to correct for the conditions.
This thesis analyzes all the already made observations of the project to create a exposure time calculator (ETC) to improve the quality and time management of future observations. A minimal exposure time based on the stellar characteristics needs to be determined and furthermore it will be investigated which adaptions should be made based on the conditions during the observations.
The result of this thesis will provide a new orientation for the observer to select a usable exposure time or to check if other projects get a usable result with the setup of the spectrograph.

Contents

1 Introduction

At the moment one of the most interesting research topics in astrophysics is the search for exoplanets. Exoplanets are planets like the Earth, Jupiter or Mars orbiting around other stars but very hard to detect because they are not self luminous and we rely on the star to find them. Therefore the first exoplanets were only detected in 1989 as a possible giant planet ($11 M_{\mathrm{J}}$) around a solar type star by Latham et al. [1989]. Until today there were discovered and cataloged around 3525 (11.09.2016) (web [a]) of these exoplanets. The ultimate goal of this search is the finding of a second 'earth' in the habitable zone around a sun-like star where life as we know it could exist.
There are a few different methods of searching for these planets. The transit photometry method measures the decrease in flux of a host star caused by a transiting companion, while the pulsation timing method measures the difference in timing caused by a change in distance of periodic pulses and the astrometry method which will be used by the GAIA space-based search. But the most common one which was also used by Latham et al. [1989] is the radial velocity method based on the doppler shift from the movement of the star and exoplanet around their common center of mass (see Fig. 1.1):

$$\Delta\lambda = \pm\frac{v_r \lambda}{c} \tag{1.1}$$

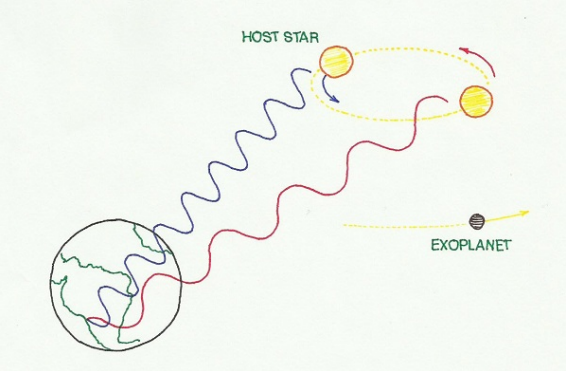

Figure 1.1: Doppler effect with shift of wavelength(web [f]) caused by the movement of the exoplanet around the star and together around their center of mass

The wavelength shift can be measured by spectroscopic observations and with repeated observations the radial velocity [Cumming et al., 1999][Clubb, 2008] can be fittet by:

$$v_{\mathrm{r}}(\varphi) = K \times [\cos(\varphi + \omega) + e \times \cos\omega] + V_{\mathrm{r}S} \tag{1.2}$$

with $V_{\mathrm{r}S}$ as the system motion, the eccentricity e, φ as the angle between the planet and the star, ω as the deviation of φ and the all important velocity semi amplitude:

$$K_\star = \left(\frac{2\pi G}{P}\right)^{1/3} \frac{M_{\mathrm{p}} \sin i}{(M_{\mathrm{p}} + M_\star)^{2/3}} \frac{1}{\sqrt{1-e^2}} \tag{1.3}$$

with the gravitational constant G, the mass of the star $M_\star$, the planetary mass M_{p}, the inclination angle i of the planet and the orbital Period P which is by Kepler's law related to the orbital radius and the mass of the star:

$$P^2 = \frac{4\pi^2}{G(M_\star + M_{\mathrm{p}})} \times a_\star^3 \tag{1.4}$$

So it is only logical to look at the most common and low mass stars in our universe for the exoplanet search. Around 75% of all the main sequence stars are M stars and especially the M-dwarfs fulfill our requirement of low mass with only up to $0.60 M_\odot$ [Reid and Hawley, 2005] and their low temperature means that the habitable zone is not far from the star which leads to a small a.
The habitable zone is mainly the area around a host star where the atmosphere of a planet can keep the water in a liquid state over a long lifespan of the star which favors the search around M-dwarfs because of the low temperature of the star which leads to a habitable zone in close vicinity of the star. Due to the close orbit and the low mass the rotational period (Eq. 1.4) of the exoplanet is only up to a few weeks so that after a short amount of time of observing the first conclusions can be taken. But one problem is that these dwarfs emit most of their light at the long visible

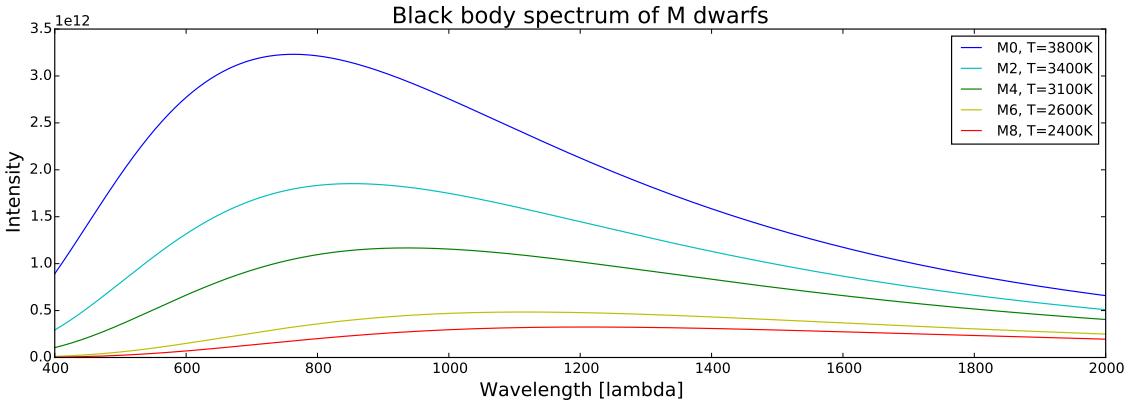

Figure 1.2: Black body spectrum of different M stars with different temperatures

wavelengths and the near infrared regime (see Fig. 1.2) and are especially hard to observe in the near infrared from Earth because of the absorption from our atmosphere. Another problem is the low luminosity of these stars therefore long exposure times are needed to get a sufficient signal.
Therefore CARMENES (**C**alar **A**lto high-**R**esolution search for **M** dwarfs with **E**xo-earths with **N**ear-infrared and optical **É**chelle **S**pectographs), a consortium of eleven Spanish and German institutes, uses two different spectrographs at the 3.5m telescope in Calar Alto (Spain) to observe a carefully chosen selection of 300 M dwarfs. The 300 chosen M dwarfs were categorized into samples of 100 early types M0-M2 (S3), 100 mid types M3-M4 (S2) and 100 late types M4 and later (S1) to study the planetary population around the different types.
The target fibre of the telescope has a field of view of 1.5 arcesc and after the fibre the light gets divided by a beam splitter to be sent into two seperate Échelle spectrographs simultaneously. Then a 4k x 4k CCD covers the wavelengths from 0.52-1.06 μm in the Visual and two 2k x 2k HgCdTe detectors for the wavelengths from 0.96-1.71 μm in the near infrared with spectral resolutions $R = \lambda/\delta\lambda$ of 95000 and 80000. Until the end of 2018 the project will search over 600 nights for exoplanets in the habitable zone around their host via the radial velocity method with an error of around or even better than 1 m/s.
At the moment the S1 sample can only be observed by CARMENES, S2 can be observed very efficiently in the near infrared and will be used for cross checking with other surveys and S1 are very bright targets which can also be observed during bad nights [Kim, 2015].
Additionally it will be possible to make a statements about the activity of the stars by analyzing different spectral lines like the calcium infrared triplet [Brinkmoeller, 2016].

2 Motivation

To optimize the time management and the overall quality for CARMENES the exposure times of the observations should be as short as possible while also achieving only a small radial velocity error. This RV error highly depends on the precision of the spectrograph calibration and the signal-to-noise ration (SNR) of the observation. The calibrations are done every night with the emission lines of different spectral lamps for long term stability and the grid of a Fabry-Pérot etalon for the short term stability over the night. But the SNR can change even for the same star on back to back observations. Changing observation conditions cause a drop in the flux and can only be countered by the exposure time of the target:

$$t \propto SNR^2 \tag{2.1}$$

The dependencies between the conditions and the exposure time have to be worked out with the help of the information saved in the ".fits" files of previous observations. These files contain all the information of the detector read out and additionally the observation parameters are saved in the so called header.
Our goal is it to find the dependencies of the stellar characteristics and the observation parameters on the SNR and exposure time to provide the observer with a tool to calculate the required exposure time for any desired observation by fitting the used exposure time in combination with the achieved SNR in varying conditions using the already available CARMENES observations.

$$EXPTIME_{calc} = t_{exp}(J) \times f_{see}(see) \times f_{air}(air) \times f_{other} \tag{2.2}$$

This will be the so called exposure time calculator (ETC).
For a typical ETC like the one for HARPS the interface consists of some kind of target information. Normally the target could be any kind of star so the input covers a few different models but we will most likely only need something similar to the black body spectrum with the target magnitude:

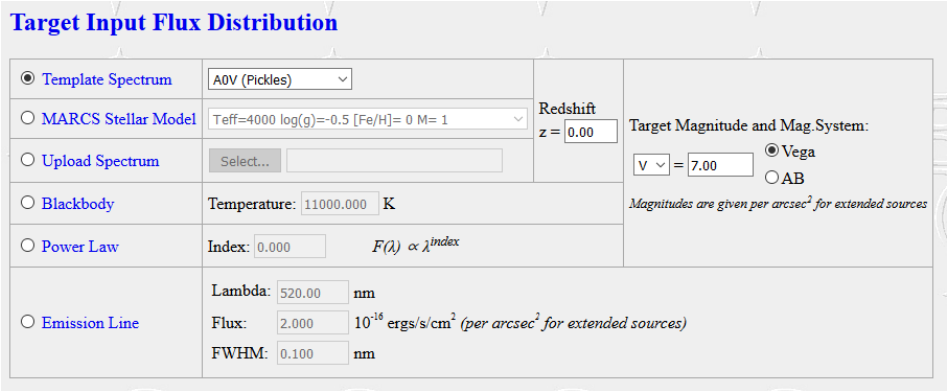

Figure 2.1: Example of the HARPS ETC target Information

Additionally a few important sky conditions, most importantly the seeing and air mass, are needed on which the exposure time and SNR can depend on:

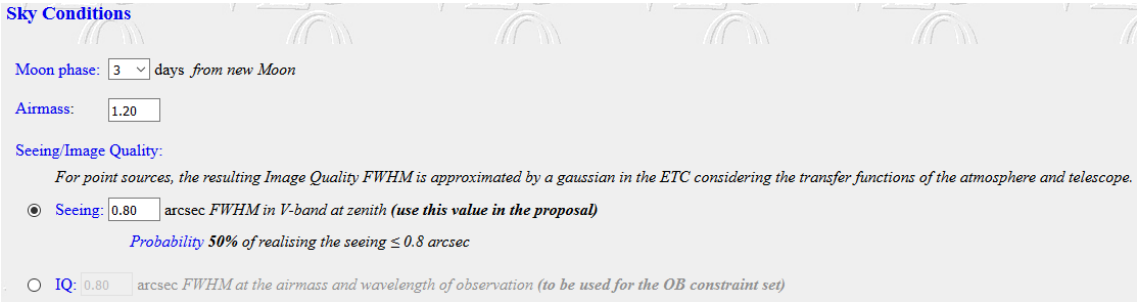

Figure 2.2: Example of the HARPS ETC observation conditions

And in the end a selection of output information with later direct output or for us it would be sufficient to directly give back an exposure time and if the time exceeds the maximum exposure time of 1800 s a prediction of the SNR:

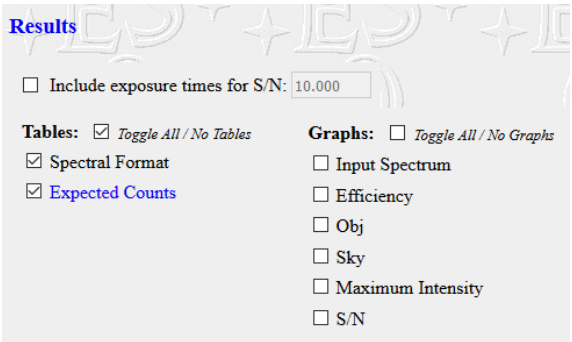

Figure 2.3: Example of the HARPS ETC selection of the results

3 ETC: Input and Output

Most of the data we use we get from the ".fits" files. For this analysis we only use the reduced "vis_A.fits" and "nir_A.fits" files uploaded to the Carmenes GTO archive (web [e]) till the 30.08.2016. Unfortunately since 01.07.2016 only a few of the over 600 observations were uploaded but issues with the server corrupted even these files to 0 bytes. This means the analysis for the ETC is done by a limited number of data-sets shown in Table 3.1 with the latest data-set of the morning from the 30.6 to 1.7.

Table 3.1: Number of data-sets

Channel	# of Observations	# of files	$150 \pm 20\%$	$150 \pm 10\%$
Visual	2386	1618	198	92
Near infrared	1758	1127	338	155
Simultaneous	1748	894	...	...

The number of observations are based on the table of M. Brinkmöller [Brinkmoeller, 2016] which was last updated on 23.8.2016 and counts multiple observations, with sometimes over 10 back to backs as one(web [k]). The list still includes canceled observations due to guiding issues or other problems.
The used data is mostly written into the header of the "*.fits" files and provides us with the SNR by order calculated by the CARACAL pipeline with the FOX method [Zechmeister et al., 2014] [Zechmeister, 2015] and the important observation parameters. The FOX algorithm takes the central n = 100 pixels of the detector and calculates the SNR by:

$$SNR = \sqrt{\frac{1}{n}\Sigma_x \frac{r_x^2}{\varepsilon_{r_x}^2}} \tag{3.1}$$

with r_x as the best fitting amplitude to each spectral bin x and $\varepsilon_{r_x}^2$ as the variance of r_x. For the stellar characteristics our reference is the alpha star list (web [d]) and additional information for the seeing and weather are taken from the nightlogs in the Redmine wiki (web [i]).
First of all we need to find the relation between δRV and the SNR. After that we can calculate a first time estimation with one or both the stellar characteristics and then apply the dependencies for the observation parameters one by one (Eq. 2.2). Most important for this are the seeing, air mass, extinction and weather. The goal

is that the ETC can reproduce the exposure times of the old observations. This allows to predict the required SNR for $\delta RV = 1m/s$ for future observations.

3.1 Relation of δRV to SNR

3.1.1 δRV vs SNR

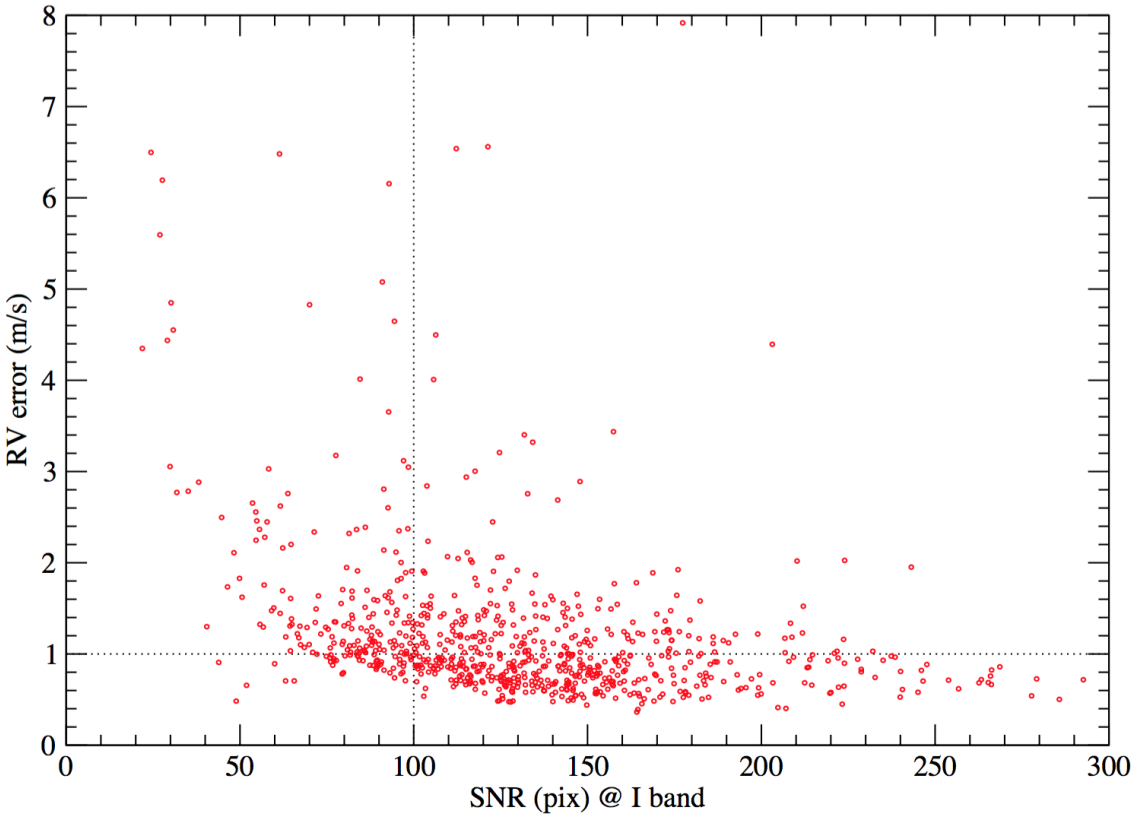

Figure 3.1: Relation between the total δRV and the SNR in I-Band (Order 46 in the Visual) to select the required SNR for $\delta RV = 1m/s$
dotted lines indicate Ribas's assumption that SNR = 100 leads to $\delta RV = 1m/s$ by Ignasi Ribas, 2016-06-08 (web [g])

According to Ignasi Ribas's plot in Fig. 3.1 it is a reasonable assumption that a $SNR = 100$ at I-Band (order 46, $\approx 8500\mathring{A}$) relates to $\delta RV = 1m/s$(web [g]). However this analysis was done around the maximum SNR for the VIS channel (see Fig. 3.3) but we need an acceptable result over a wider range of orders. Therefore we take a look at the median SNR without the first 10 orders with very low SNR and the last 6 orders which are a result of the beam splitter and do not represent the stars spectrum and compare it to the SNR in order 46 (see Fig. 3.2).
The linear fit shows us that a median SNR of around 130 would be a sufficient value to get $\delta RV = 1m/s$ over half of the relevant orders. To get an even more precise result, deviations still being in the vicinity of $1m/s$, variations in the relation of median to order 46 and as agreed with the instrument astronomer J. Caballero we

set the threshold SNR up to 150 (around 120 in order 46).
Given that there is still some work to be done on the δRV calculation and precision of the NIR channel and no assumptions for the correlations of SNR to δRV have been made so far the required SNR will also be set to 150 there for this thesis but should easily be changeable for later calculations.

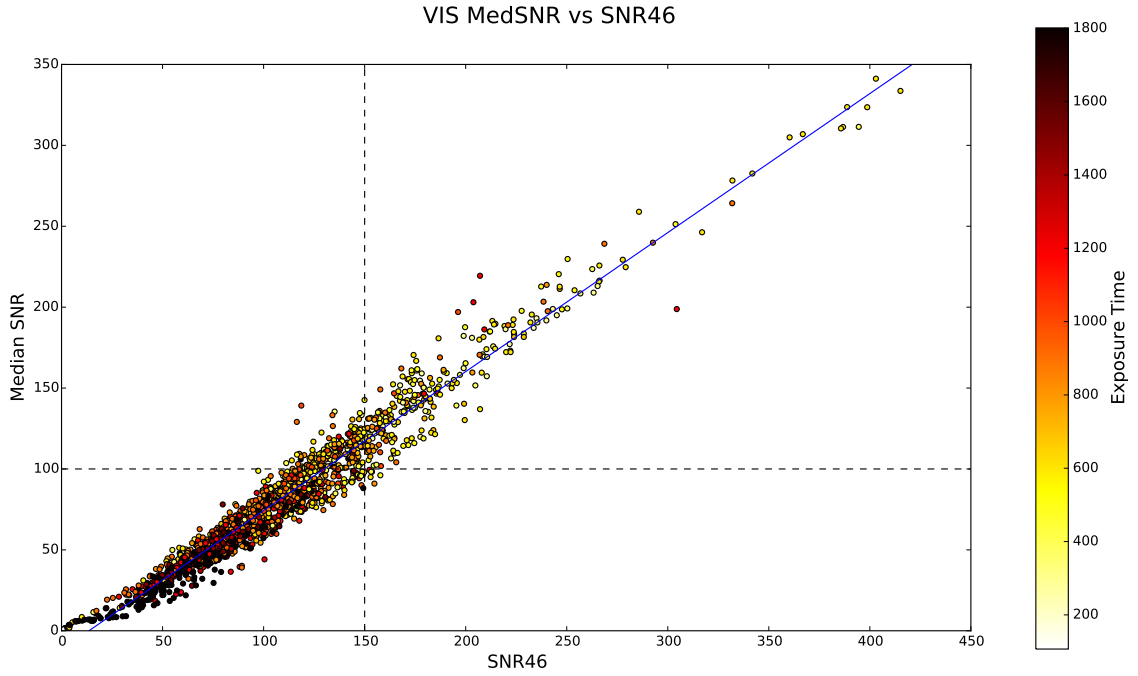

Figure 3.2: Relation between the median SNR and the SNR in order 46 of all observations with a linear fit with offset to select a suitable SNR for the calculations, the horizontal line shows Ribas's assumption of SNR = 100, the vertical line our choice of SNR = 150

3.1.2 VIS vs NIR

The spectra of the VIS and NIR are as said in the introduction taken with two different spectrographs and detectors, so there are some differences observable. The two combined spectra of Luyten's star (see Fig. 3.3) as a representative for all stars (see Fig. 3.4) show higher SNR values in the NIR than in the VIS channel caused by the higher flux in the J band (NIR) than in the I band (VIS) and therefore we should expect longer exposure times for the VIS.
This is supported by Fig. 3.4 which shows all combined simultaneous spectra with nearly every NIR median higher than their VIS counterpart and additionally illustrates that there might be a connection to the spectral type (SpT) supported by the look at the black body spectra (see Fig. 1.2) but it could also be that this effect can be handled by the $t(J)$ calculations and so it needs to be checked later.
Also shown (Fig. 3.3) is the increasing SNR distribution over the VIS with the plateau in the NIR as expected for M-dwarfs and for which the project is optimized. It is also obvious that it will not make a great difference if we use the median or

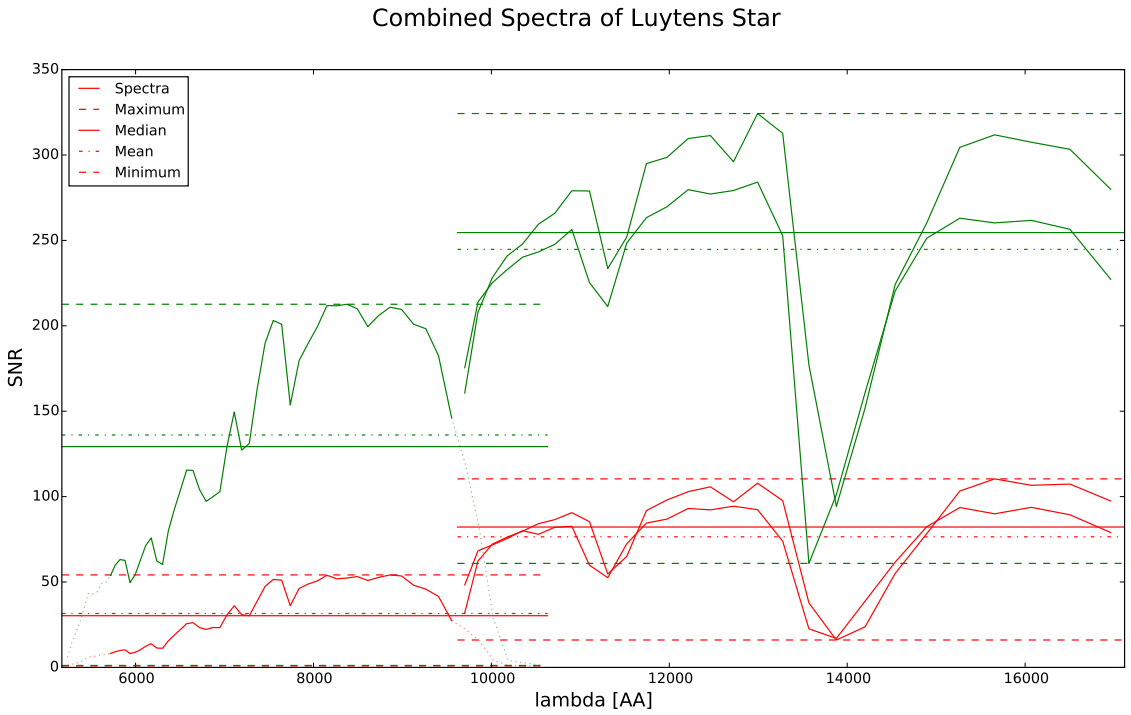

Figure 3.3: A high (green) and a low (red) SNR spectrum of Luytens's star to illustrate the characteristics of the spectrum and the differences and causes of the min, max, median and mean values for the VIS and NIR channel

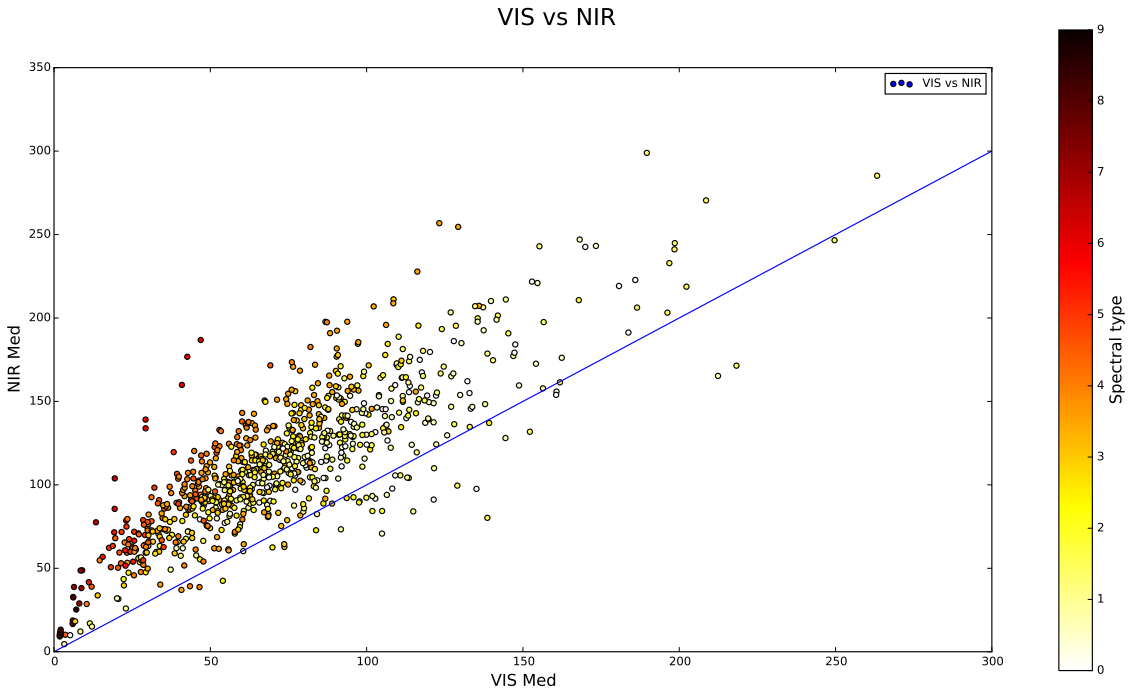

Figure 3.4: The relation between the median of the VIS and NIR channel for observations with both data-sets for the same observation present color coded with the SpT to illustrate the dependency on temperature

the mean for the calculations so we stay with the median.
Furthermore the NIR channel has two obvious features. First it consists of the two mentioned detectors for the same wavelength range which results in two slightly different spectra and second the dips around 11400$\mathring{A}$ and 14000$\mathring{A}$ are caused by strong telluric absorption lines from gases like carbon dioxide in the atmosphere (web [h]).

3.2 Stellar characteristics

The most important input for the ETC are the stellar characteristics because they provide us with an initial observation time. We are provided with two parameters, the J band magnitudes (J) and the spectral type (SpT). First of all both parameters have to be checked separately but we have to keep in mind that there can also be connections between both and the dependency, like already seen in Fig. 3.4, on a parameter has to be considered in the analysis.

3.2.1 J band magnitude

Fig. 3.5 shows a clear correlation between the median SNR, J and also between the exposure time in both channels. It is obvious the longer the exposure time for one star becomes the higher the median SNR can get and for the same median SNR we need to increase the exposure time the fainter the observed star becomes.

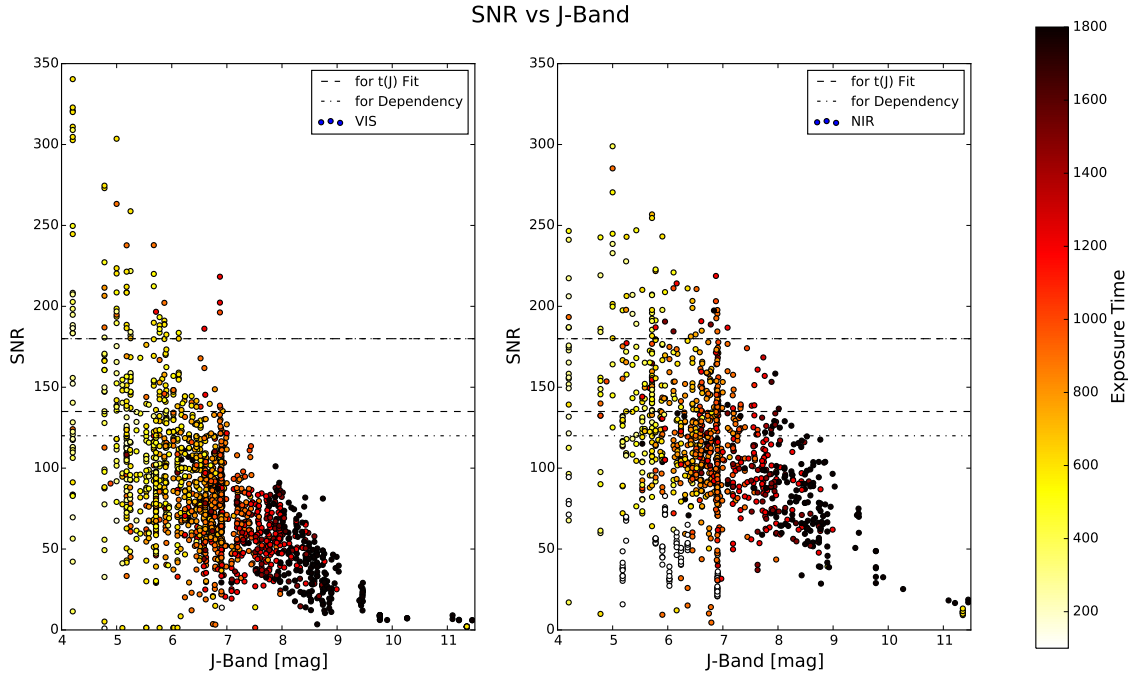

Figure 3.5: Median SNR vs J band and the limits for the data-sets later used for the lower envelope fit(upper: 150+20%, lower: 150-10%) to calculate the initial exposure time and for the search of dependencies of the observation conditions on the exposure time(upper: 150+20%, lower: 150-20%) (left: VIS, right: NIR)

This means we have a clear correlation between the magnitude of the star and the SNR and it can be explained by the connection of the SNR to the number of photons N:

$$SNR = \frac{N}{\delta N} = \frac{N}{\sqrt{N}} = \sqrt{N} \tag{3.2}$$

The magnitude in J can be calculated by the relation of the luminosity of our sun($L_\odot$) to the star(L). The luminosity is also connected to the flux f and therefore to the photon number N:

$$J - J_\odot = m - m_\odot = -2.5log\frac{L}{L_\odot} = -2.5log\frac{f}{f_\odot} = -2.5log\frac{N}{N_\odot} \tag{3.3}$$

This means J is related to a constant and N:

$$J = J_\odot - 2.5logN + 2.5logN_\odot = const - 2.5logN \tag{3.4}$$

After a short transposition to N:

$$N = 10^{\frac{const - J}{2.5}} = e^{\frac{A - J}{B}} \tag{3.5}$$

we can include Eq. 3.5 into Eq. 3.2 and get the theoretically expected dependence of the achieved SNR on the J band magnitude:

$$SNR(J) = e^{\frac{A - J}{2B}} = e^{\frac{A}{2B}} e^{\frac{-J}{2B}} = const \times e^{-C \times J} \tag{3.6}$$

with A, B, C as constants.

In the VIS Fig. 3.5 shows a lack of observations above J=7 mag and exposure times higher than 1200s (red to black points) in a considered range of SNR 150 (+20%,-10%) for our initial exposure time calculation which will lead to an unverified result for fainter stars. Additional concern is caused by the lack of further fainter stars and longer observation times for the dependencies on the observation conditions.

However the NIR has observation times up to the maximum of 1800 s in the considered calculation range and because of the higher flux even stars up to J=8 mag and fainter for the analysis of the dependencies. The few white 100 s exposures in the NIR around J=5.2 mag, 6.9 mag and a group of different stars around 6 mag are accidentally splitted long term observations of one night.

3.2.2 Spectral type

A similar relation as the one in J is present for the SpT but not that clear cut (see Fig. 3.7). At first Fig. 3.7 looks a bit chaotic but on the second look the same SNR vs exposure time is visible but shifted around. The big problem is the distribution of different continuous J into a few discrete SpT as shown in Fig. 3.6 but not sorted by brightness but by temperature. For example around J=7 mag the stars can be put into SpT from M0 up to M6 and for M1.5 the J range is from the brightest star at 4.203 mag up to 7.5 mag which has an big impact according to the J relation in Eq. 3.6. This means we can not use the SpT for the initial exposure time calculation but have to search for a dependency factor later like the one we already hope to find for the NIR channel (Fig. 3.4).
The dependency is caused by the temperature of the star which influences the emitted black body spectrum (see Fig. 1.2) and shifts the maximum of the spectrum from the visible red wavelengths to the near infrared. Therefore a J=7 mag M0 star should need less exposure time in the VIS because of the higher flux than a M4 star with the higher flux shifted to the near infrared.

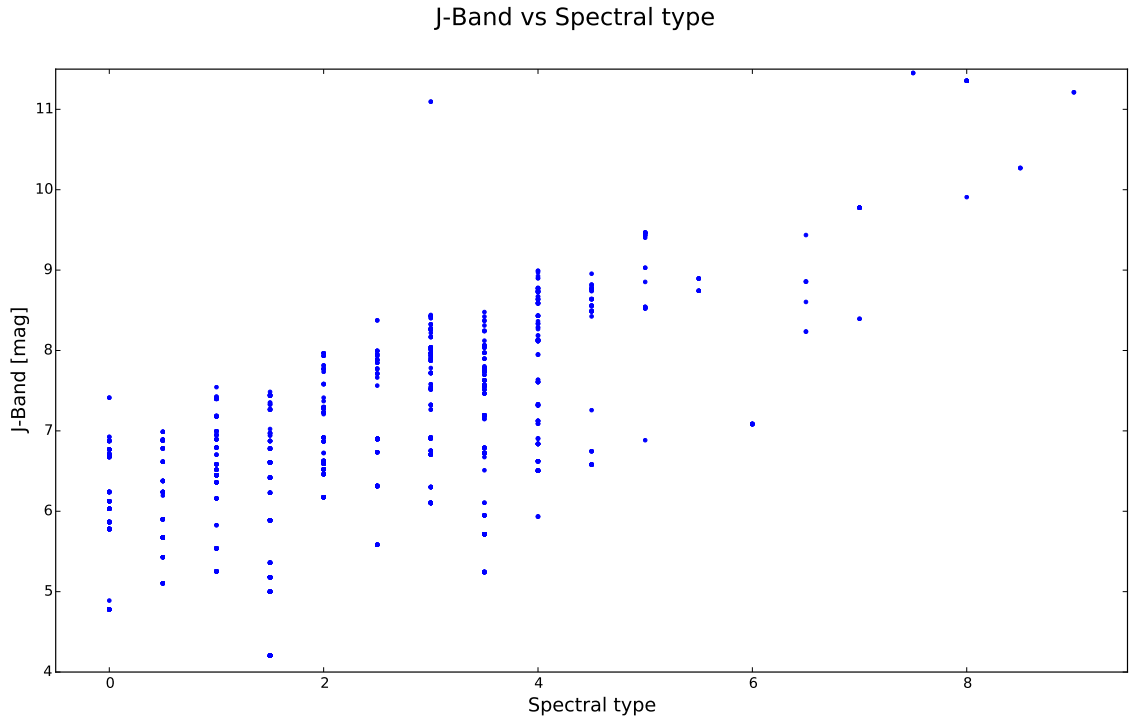

Figure 3.6: Relation of J band and spectral type

A special note goes to the M3, J=11 mag star K2-33 which is not included in the alpha list (web [d]) or any sample group and far off the other targets around 11 mag and M3 but the recent finding of a young super Neptun (web [c]) made the star an additional target to observe.

Fig 3.7 illustrates that for the VIS we only have a good sample of observations for M0 to M1.5, up to M3.5 we lean towards lower SNR and afterward there is nothing to analyze anymore. So it will be highly unlikely that the analysis will show a meaningful dependency. On the other hand the NIR supplies us with a good selection of observations up to M3.5 and with a few wide spread data-sets up to M6. Thus we might find a suitable dependency to include the SpT into the calculation of the NIR exposure time and thereby explain Fig. 3.4.

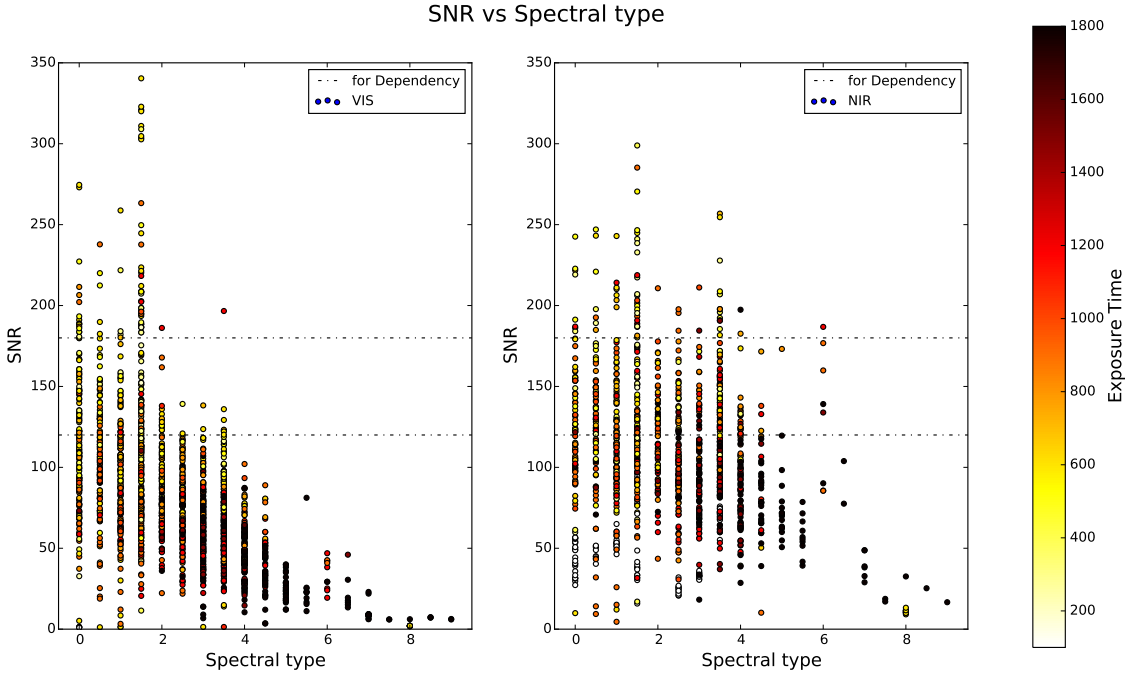

Figure 3.7: The median SNR vs SpT and the limits ($150 \pm 20\%$) for the analysis of the dependency of the temperature on the exposure time(left: VIS, right: NIR)

3.3 Seeing

The first and hopefully significant contribution comes from the seeing and here it already starts to become complicated. The seeing is caused by turbulence in the atmosphere moving bubbles of air around and therefore break the initially plane wave front so that a telescope registers varying intensities for one wave front. So during a long observation the seeing causes the target to wiggle around the center and therefore the optimal point distribution with sharp edges transforms into a normal distribution. The worse the seeing becomes the wider the distribution gets and this can be a big problem because the hole for the fiber of CARMENES is only 1.5 arcsec in diameter. The seeing itself is given as a FWHM value ($\approx 2.355\sigma$) so that for a seeing of 1.5 arcsec it already means around 25% of the light should be lost. An example for different seeings and what the fiber would catch is illustrated by Fig. 3.8.

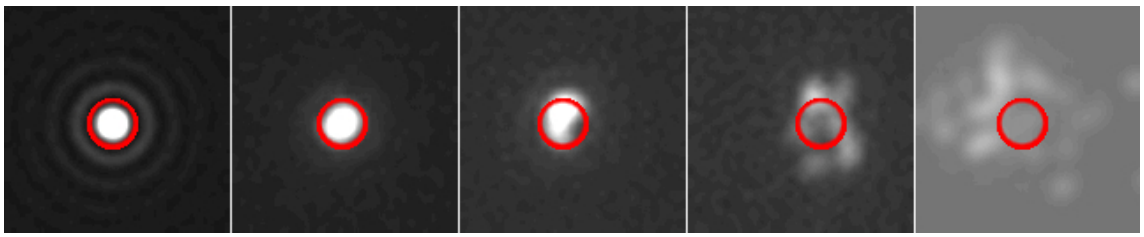

Figure 3.8: Example for different seeings and what the fibre (red circle) would see(web [j])

For a precise analysis the data in the header from the seeing monitor at Calar Alto which is located outside the dome is needed but it lacks the additional dome seeing effects caused by turbulence from temperature differences inside and outside the dome. Furthermore the mirror seeing from temperature differences in the vicinity of the mirror have to be included as well as additional optical effects. The problem is that for about 2/3 of the file headers these seeing values are missing (see Fig. 3.9, 0 arcsec bin) because the monitor only works up to a relative humidity of 80% and wind speeds below 12 m/s (apparently 50% of the time) [Sanchez et al., 2007] or according to J. Caballero up to 1.6 arcsec (supported by Fig. 3.9).

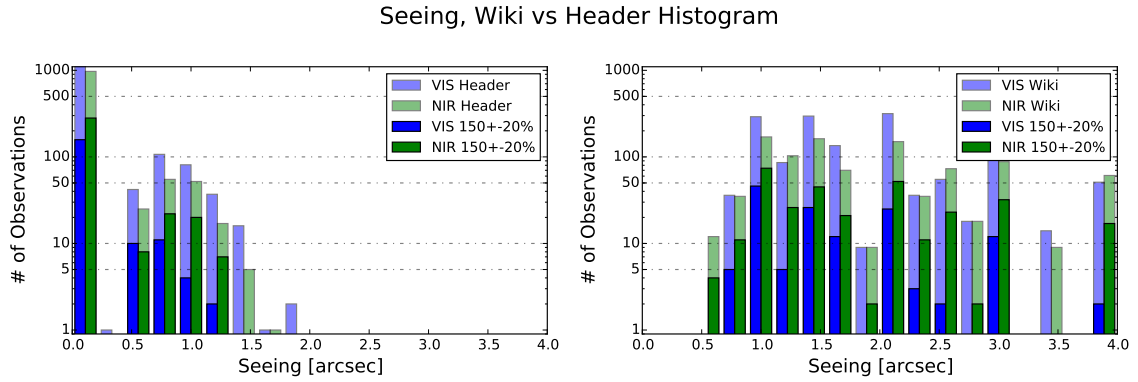

Figure 3.9: Number of observations for different seeing values (lighter colors) and number used for the analysis of the dependency(darker colors) for the VIS(blue) and NIR(green)(left: header, right: wiki); 0 arcsec means no information in the header

Fortunately the observers have to note a seeing value in the Redmine wiki (web [i]) but for nearly all nights it is not mentioned how and when the value was measured. The value could be taken from the seeing monitor at one point, could be an average of a few certain points during the night and could also include a correction for some additional seeing factors already. If the seeing was so bad that the monitor never showed a value it could be a best guess or it was noted a range (2-4 arcsec) for the value where it is unclear if the observer meant it as an changing range through the night or just as an estimation.

The only good information that comes from the header seeing is the correspondence in the distribution to the long term night sky observation at Calar Alto [Sanchez et al., 2008]. The percentage increase in missing header data can be explained by the

short period from January to July in which the observation were done in comparison to the 2.5 years for Sanchez et al. [2007].

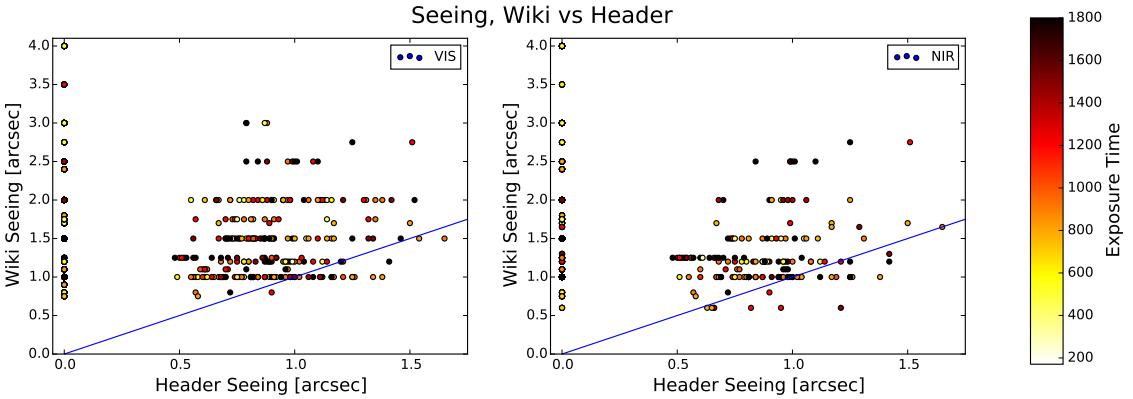

Figure 3.10: Relation between the wiki seeing and the header seeing color coded with the exposure time with linear fit for the correlation(left: VIS, right: NIR)

Fig. 3.10 shows that for the available header values no clear distribution of the wiki values is observable so there is no way to make an acceptable calculation for the missing header values. But it might suggest that for the higher seeing values the different effects of the dome seeing could be included and for the night log seeing values which correlate with the header seeing values no such thing has been done. So for better or worse we have to use the wiki seeing values if we want to derive an exposure time adjustment for the seeing which can have errors of up to 1 arcsec

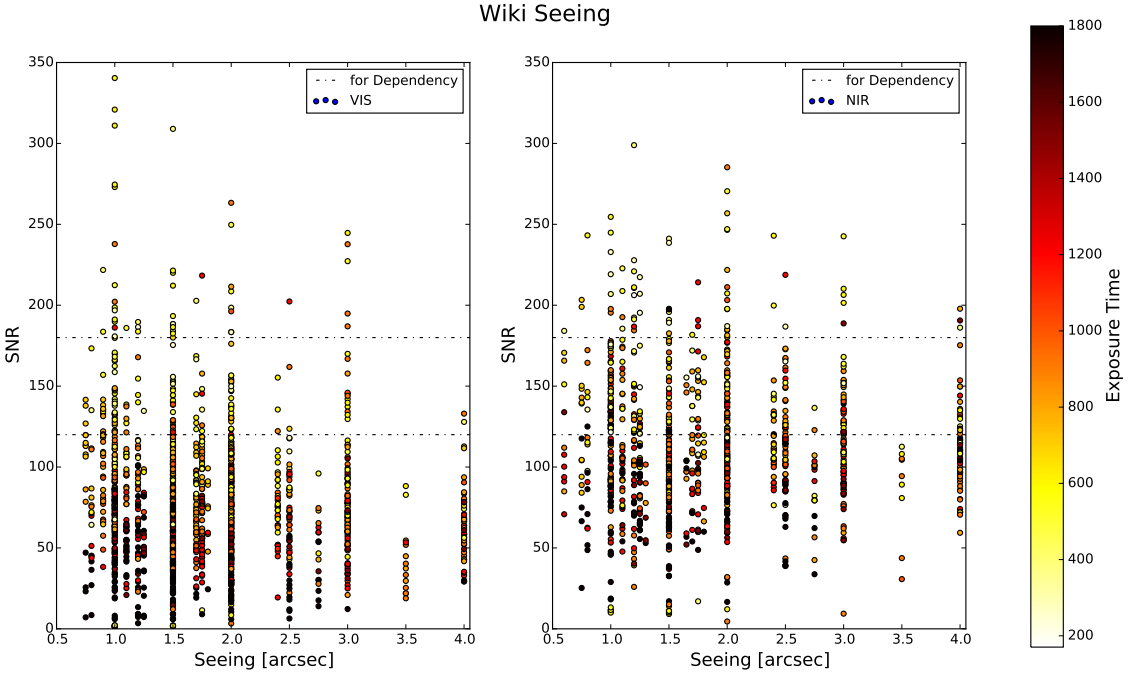

Figure 3.11: Median SNR vs wiki seeing with the limits of points looked at $(150 \pm 20\%)$ for the dependency analysis of the seeing on the exposure time color cloded with the exposure time(left: VIS, right: NIR)

(for ranges 2-4 arsec) or even higher if drastic changes or the addition of dome seeing effects were not noted in the wiki.
Yet again this means that we have to work with a more or less discrete distribution (see Fig. 3.11). For both channels we have a great scatter up to 2 arcsec seeing. However for the VIS the only other good variety of data-sets is available for 3 arcsec so the analysis fit will likely be inaccurate for higher seeings but here it is needed the most. As before the NIR has the better distribution and we only lack observations for seeing of around 3.5 arcsec and should a priori expect the better calculation.

3.4 Air mass

The second dependency comes from the air mass which is calculated by the telescope distance to the zenith (z) shown in Fig. 3.12.

$$airmass = sec(z) = \frac{1}{cos(z)} \tag{3.7}$$

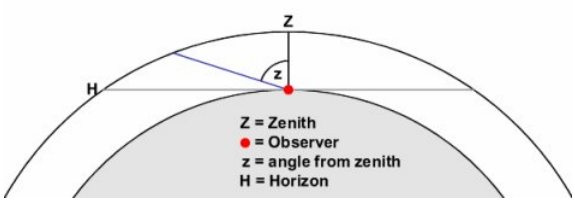

Figure 3.12: Air mass and the zenith angle

The atmosphere consists of different layers with varying thicknesses. Each layer has a different impact on a wavelength and the amount of absorption. The higher the telescope is located the better because it minimizes the amount of air mass in general and most important the air mass in the planetary boundary layer.
The planetary boundary layer is highly influenced by temperature, wind and humidity and the thickness can change constantly during day and night, summer and winter based on the conditions. To get around any further loss of flux in upper layers by scattering at particles and absorption by molecules such as for the carbon dioxid causing the strong dips in the NIR every meter of avoided air mass is important. Therefore Calar Alto is at the altitude of 2168m a decently placed observatory.
Additionally the sky gets illuminated from the ground and in some nights by bright moonlight which can slightly alter our signal of the star namely the SNR but not necessarily the δRV. All this is the reason behind the most observations around the zenith, the potential decrease in observations illustrated in Fig. 3.13 and the self set limit to an air mass of 2.

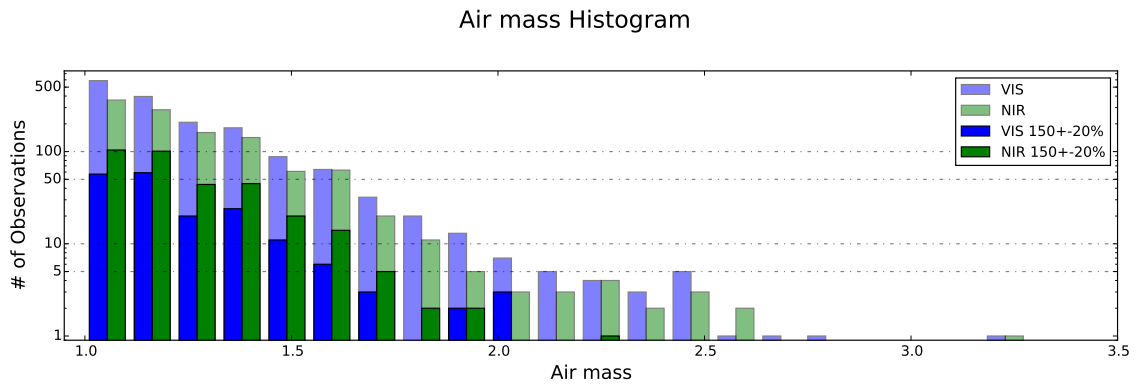

Figure 3.13: Number of Observations for different air mass values (light) and number used for the analysis of the dependency (dark) for the VIS (blue) and NIR (green)

The observations above air mass 2 were most likely of stars which moved under the horizon after the observation and are now not observable anymore for a longer period of time. Both channels lack observations above 1.7 air masses but there should be enough well spread data-sets at lower air masses for a good linear fits(see Fig. 3.14). For a telescope the extinction coefficient k (mag/air) depends on the wavelength and varies for the VIS from 0.13 for 500 nm to 0.05 for 900 nm but is far lower in the NIR with 0.015 at 1.25 μm (example from Gemini observatory at Mauna Kea web [b]) therefore we should expect a higher dependency for the VIS.

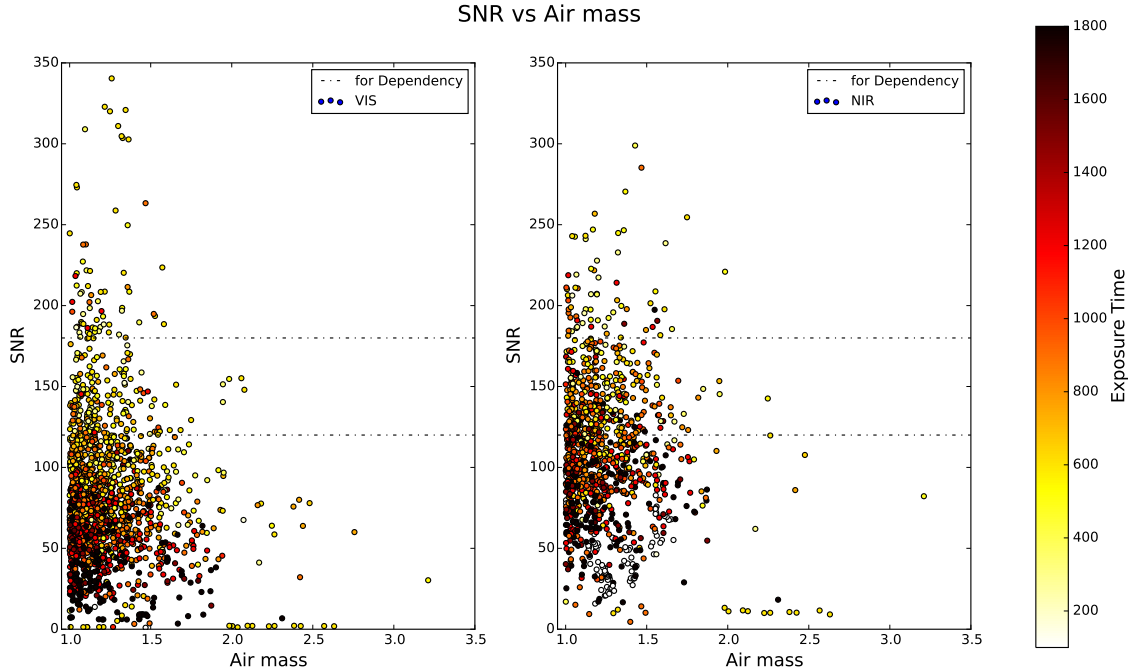

Figure 3.14: Median SNR vs air mass and the upper and lower limit for dependency analysis of the air mass on the exposure time(left: VIS, right: NIR)

3.5 Weather

Like the seeing the weather type is complicated to take into account. The only source for the weather conditions during the observations is the Redmine wiki (web [i]) with the observer entries in the night log. These entries vary from a short "photometric" to detailed information with timestamps. But again there are unclear comments like "mostly clear" or "partly cloudy" with no information what happened while it was not clear or cloudy or even when. The same goes for comments with changing weather conditions but no information when these changes happened.
So regardless of the issues the information had to be categorized as in Fig. 3.15 with the well defined types of photometric, clear, cirri and clouds. However there are still a few nights left with weather worse than just clouds as in February when observations of the brightest targets were done with "overcast" and "transparency 10-20%". These observations fall in the last category "Bad" and normally nobody would make observations under these conditions. This means again that we only have 5 discrete values to find the dependency of the weather on the exposure time.

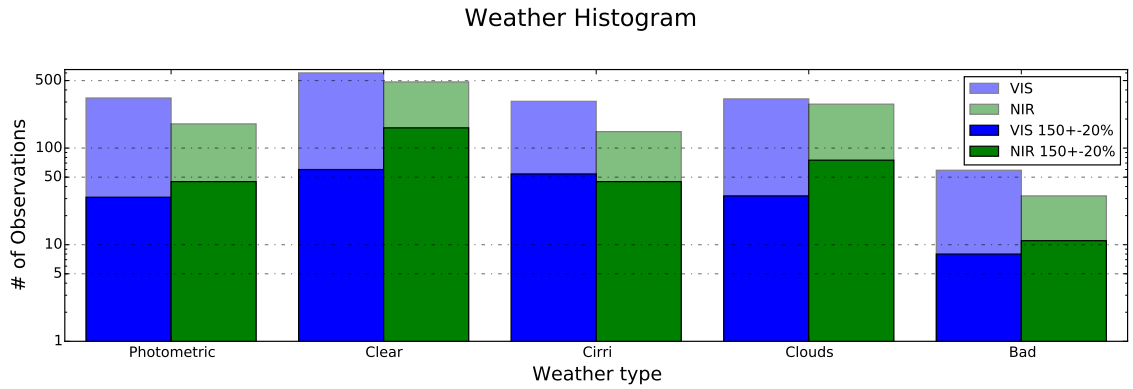

Figure 3.15: Number of Observations for the five weather types (light) and number used for the dependency analysis (dark) for the VIS (blue) and NIR (green)

The high amount of "clear" observations (see Fig. 3.15) is likely caused by chemtrails or spiderweb clouds or even short times of little haze or fog which might have caused the comments like "mostly clear". One problem with observations during cloudy nights is that it can happen that for one observation the star stays in a cloudless gap ("partly cloudy") and the SNR becomes higher than needed while during the next observation the star vanishes for almost the whole exposure time and the SNR is way too low.
Fig. 3.16 illustrates the distribution of the observations in the different weather types additionally splitted by J to further illustrate what an impact the exposure time has on SNR for the same J but different weather.

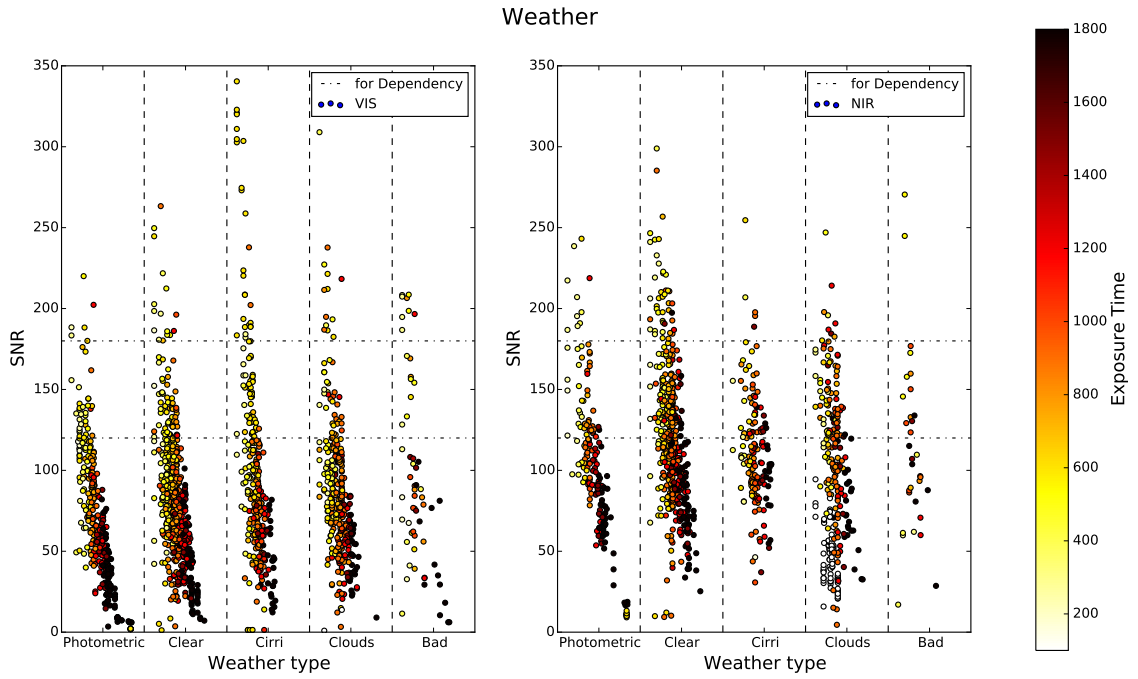

Figure 3.16: Median SNR vs weather types split up with the J band magnitudes (4 mag on the left to 12 mag on the right) in the respective weather type and the limits ($150 \pm 20\%$) for the analysis of the dependency of the weather on the exposure time additionally color coded with the exposure time (left: VIS, right: NIR)

3.6 Extinction

The Extinction is another important parameter of the observations because it reduces the flux in general but it might overlap with the air mass and weather dependencies. But similar as to the seeing the header only has the record of about 1/3 of the observations (see Fig. 3.17 values > 0).

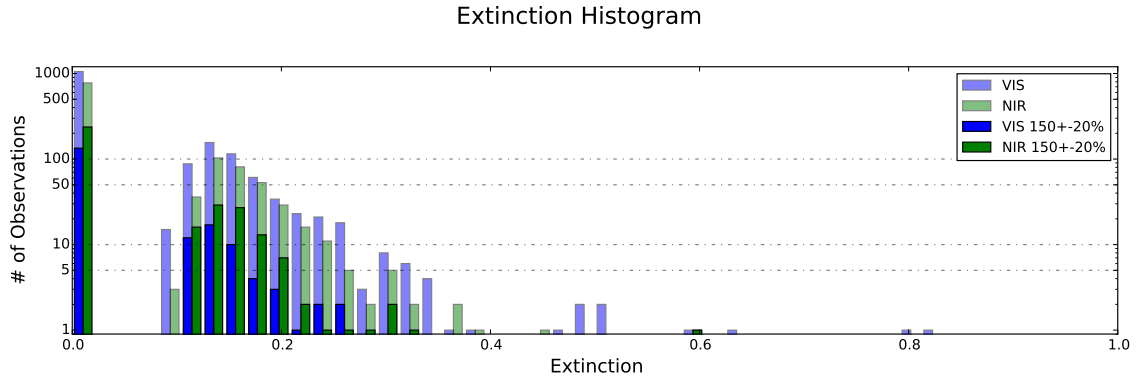

Figure 3.17: Number of Observations for different extinction values (light) and number used for search of dependency (dark) for the VIS (blue) and NIR (green); 0 means no information in the header

The bigger problem for the extinction is that the observer do not include these information into the Redmine wiki night logs (web [i]) because they vary for each observation.

By the look of Fig 3.17 and Fig 3.18 around SNR = 150 there might only be enough

good observations done around extinctions of 0.1 to 0.2 but this range is most likely to short to figure out any kind of dependency.

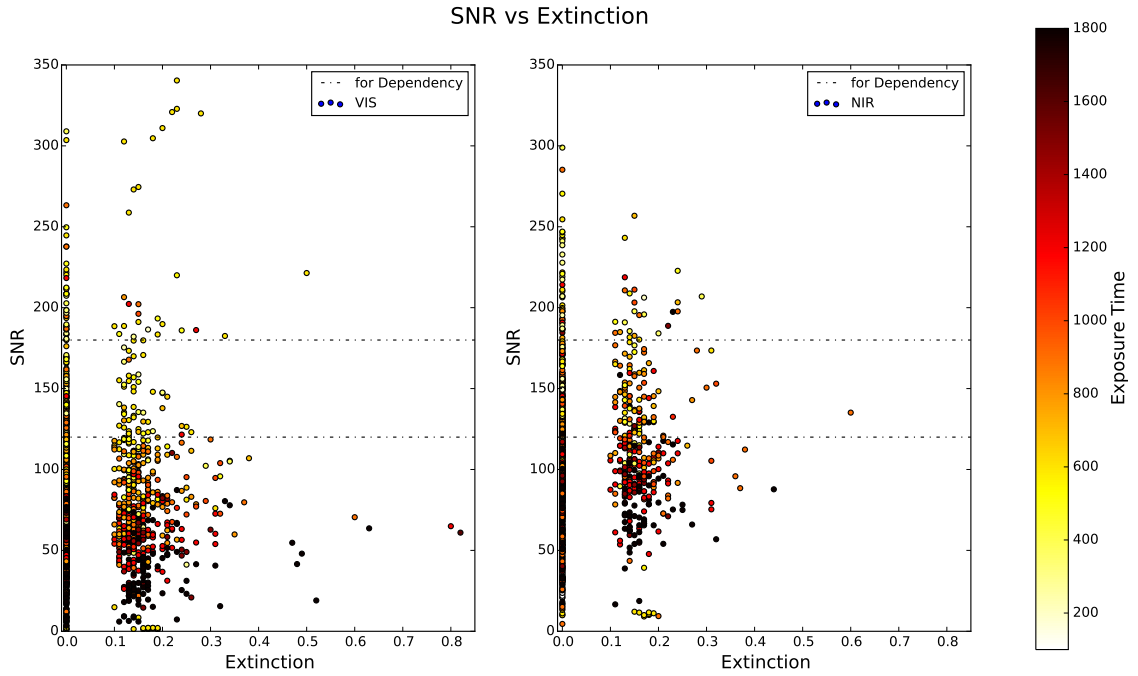

Figure 3.18: Median SNR vs extinction and the limits (150±20%) for the analysis of the dependency of the extinction on the exposure time color coded with the exposure time(left: VIS, right: NIR)

3.7 Other possible parameters

The header still contains many more possible information which can be checked but it is unclear whether the uncertainties from the other parameters allow a good analysis.

For instance could it be interesting to find out if an observation gets influenced by the overall temperature considering that we are observing all year long. Even more important would be an information about the temperature change during the observation which could cause some change in the seeing around the dome but would be impossible to predetermine for the calculation. The relative humidity could lead to changes in the extinction and absorption due to the connection to the air mass. As for the temperature the pressure itself might not be that interesting, but the change which again is not recorded could lead to some changes in the dome seeing. And at last the wind speed and direction can cause changes in air condition which lead to changes in the seeing and air mass of the boundary layer.

4 Data Analysis

The analysis will start with the connection of the SNR, J and the exposure time with Eq. 3.6 and Eq. 2.1 to get a normalized exposure time for SNR=150:

$$EXPTIME_{norm} = \frac{EXPTIME_{obs}}{EXPTIME_{calc}} \tag{4.1}$$

This normalized exposure time will be all important for the analysis of the dependency of other parameters on the time. We will look at the lower envelope for each parameter because here the other conditions hopefully only had no to little impact on the observation therefore the only reason for a too long exposure time would be the parameter itself. Therefore we apply a suitable fit to the lower envelope to get the minimal dependency and then apply it to our exposure time. After every parameter has been looked at Eq. 4.2 will be used by the ETC:

$$EXPTIME_{calc} = t_{exp}(J) \times f_{see} \times f_{air} \times f_{weather} \times f_{other} \tag{4.2}$$

with the functions derived from the data in the following sections.

4.1 J band vs SNR vs Exposure Time

To get a first minimal exposure time we need a lower envelope of the selected data with SNR = $150 + 20\% - 10\%$ (see Fig. 3.5). The lower envelope was chosen because on those points the other conditions should have had theoretically the lowest impact during the observations otherwise the SNR would have been lower or the exposure time higher to compensate for that factor. The equation for the fitting is given by EQ. 3.6 and Eq. 2.1:

$$t_{exp} = const \times e^{-C \times J} = m_{\mathrm{J}} \times e^{-c_{\mathrm{J}} \times J} \tag{4.3}$$

We started the fitting process with all the useful data (blue points in Fig. 4.1) and then removed 90% of the points one after the other. The removed points were selected by the positive residuals and a small weighted absolute residual like the one blue point in VIS around $J = 7\,\mathrm{mag}$ to ensure the overall curves look similar for the VIS and NIR. It was over all difficult to find a good final number of points for the fit and the weighting to remove the right outlier points below the fit to make the

resulting exposure time functions for the VIS and NIR fairly similar and not cross each other. The biggest problem was the progression of the curve for the exposure time of fainter stars. Because of the lack of suitable long time observations we did not have enough information about the development of the curve for the VIS and the fit tended to lower exposure times for the VIS than for the NIR.
After the initial calculations we had to take into account that we used points with different SNR so the curve got shifted to the wanted SNR of 150 with the median SNR of the used points (yellow points in Fig. 4.1) and a first result is that for stars with $J > 8.25$ mag we will always need the maximum exposure time. The resulting coefficients for the functions (Eq. 4.3) were:

Table 4.1: The coefficients of the function

Condition	Vis	δVIS	NIR	δNIR
m_{J}	15.379	2.794	16.007	2.100
c_{J}	0.575	0.029	0.561	0.019
SNR_{med}	145.390	11.910	151.025	12.444

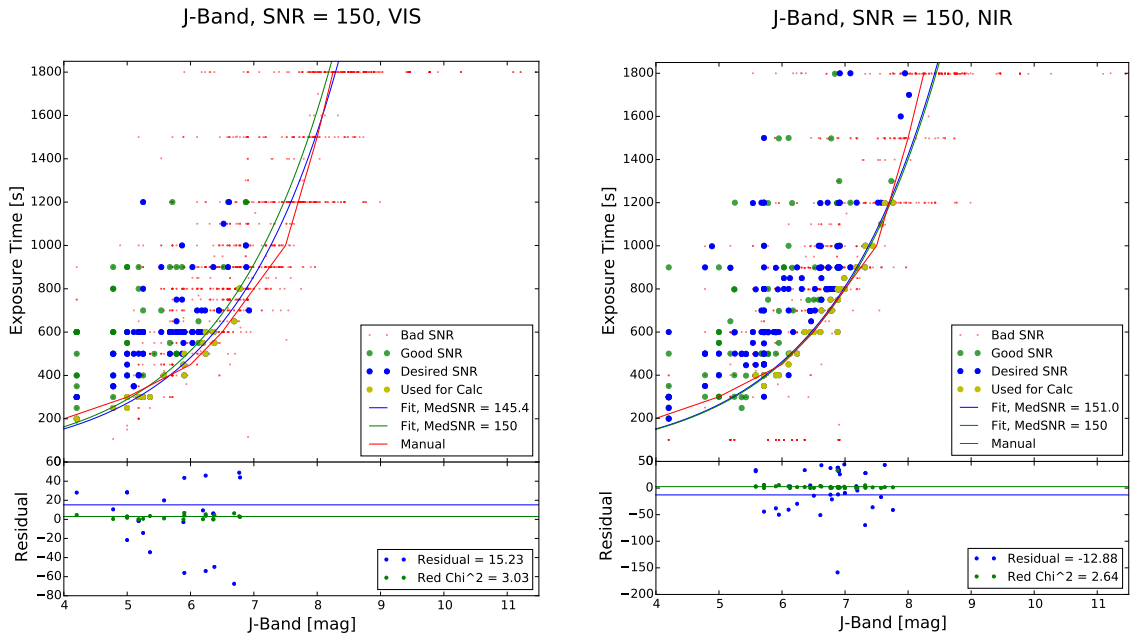

Figure 4.1: Top: Exp. Time vs J band (left: VIS, right: NIR), lower envelope fit (blue line) with the selected 10%of data (yellow points) of all the observations with $SNR = 150 + 20\% - 10\%$ (blue points), correction to $SNR = 150$ (green line) with the median SNR of the selected points (yellow), the exposure times of the observation manual (red line), observations above $SNR = 150 + 20\%$ (green points), observations below $SNR = 150 - 10\%$ (red points)
Bottom: residuals of the lower envelope fit, and χ^2_{red}

Fig. 4.2 visualizes the resulting normalized time which will be used for the first dependency analysis. With the exception of the splitted 100s observations in the NIR and some outliers there seems to be a upper and lower envelope over the whole

range of J. Our data sets for the analysis of the dependencies (blue points) lies in a tight packed segment without big outliers except a few low points in the VIS around $J = 5\,\text{mag}$ so the further analysis should get us a few good results.

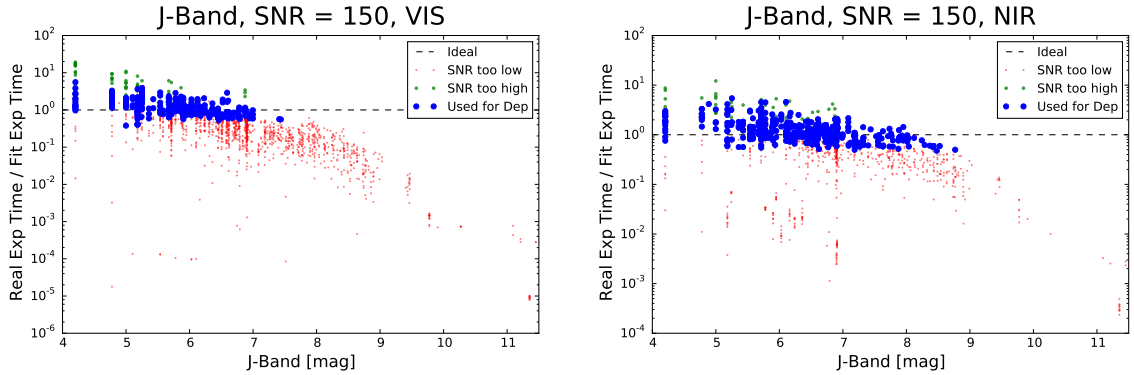

Figure 4.2: Result of the t(J)-fit displayed with norm. time vs J, observations within $SNR = 150 \pm 20\%$ (blue points), observations above $SNR = 150 + 20\%$ (green points), observations below $SNR = 150 - 10\%$ (red points)

4.2 Seeing

Because of the issues mentioned before in Ch. 3.3 the seeing was difficult to analyze. First of all in the VIS only two data sets for seeing higher than 2 arcsec were in a reasonable area for the analysis of the dependencies (see Fig. 4.3 left) and therefore we had to look at the NIR to find a suitable function that could explain the potential decrease in flux input.

There we can see a clear potential increase for higher seeing values but also the problem of the discrete allocation of points and it was difficult to find the right amount and location of data sets for the fitting process. We used the same procedure as for the $t(J)$-fit to remove 90% of the points with the help of the residuals for our fit function:

$$f_{see} = c_{see} \times e^{see} + b_{see} \tag{4.4}$$

In the end we used this exponential function which will not explain the difficult relation of the distribution function being cut off by the fiber where the star might not even be completely centralized so that the distribution is spread uneven over the fiber. But the possible errors of the seeing values itself might outweigh this problem and in the end the function gives a suitable fit which needs to checked again before future recalculations.

However this is still a function which can improve the quality of future exposure time calculations and even if it is too high the next recalculation of the factors will

hopefully have more observations in the selected range and it is possible to get a better fit then. So the important resulting coefficient is c_{see}:

Table 4.2: The seeing coefficient

Condition	Vis	δVIS	NIR	δNIR
c_{see}	5.660E-3	1.188E-3	7.246E-3	0.809E-3

The fits (see Fig. 4.3) for the VIS and NIR are as expected from a percentage loss of flux very similar and might have been the same if my reduction algorithm had included only the lower point at 4 arcsec in the NIR.

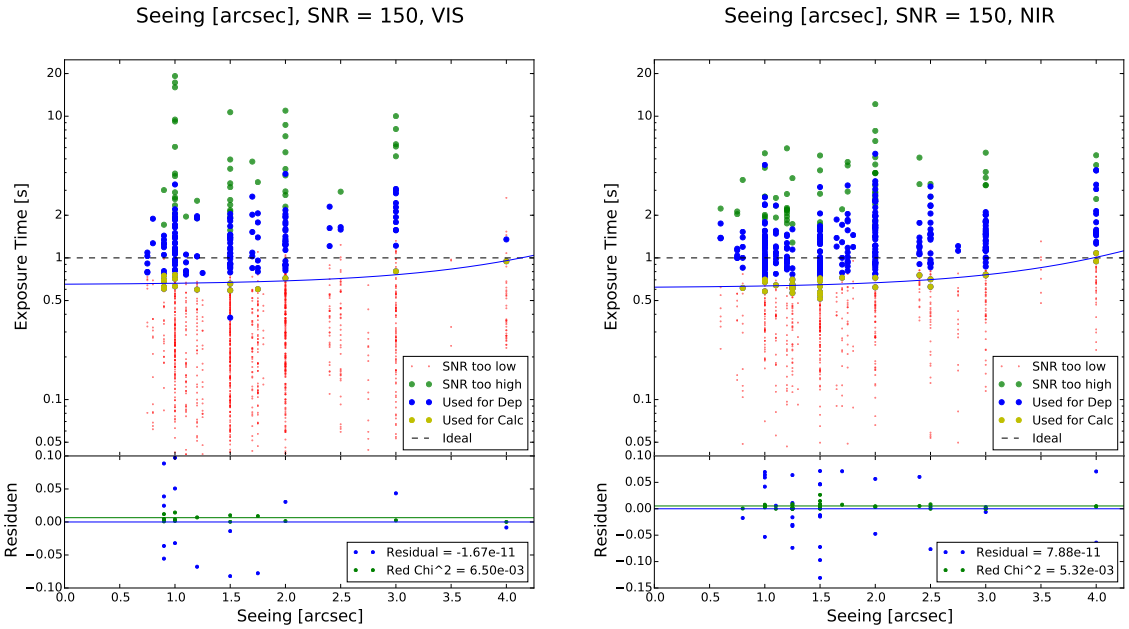

Figure 4.3: Top: Norm. time vs wiki seeing, lower envelope fit (blue line) with 10% data (yellow points), observations within $SNR = 150 \pm 20\%$ (blue points), observations above $SNR = 150 + 20\%$ (green points), observations below $SNR = 150 - 10\%$ (red points), Bottom: residuals of the lower envelope fit, and χ^2_{red}

4.3 Airmass

After the seeing correction, we had to go on with the air mass. For both channels the linear lower envelope was easily spottable without the one outlier in the VIS still remaining far off from the other observations (see Fig. 4.4). Also obvious was the expected slower increase for the corrections for higher air masses and the later support by the linear fit for the NIR.

The fit was done again with initially all points within our 20% range around SNR 150 and then reduced down to 10% by looking only at the positive residuals except

the one outlier in the VIS:

$$f_{air} = b_{air} + c_{air} \times air \tag{4.5}$$

with the important coefficient c_{air}:

Table 4.3: The air mass coefficient

Condition	Vis	δVIS	NIR	δNIR
c_{air}	0.561	0.076	0.030	0.037

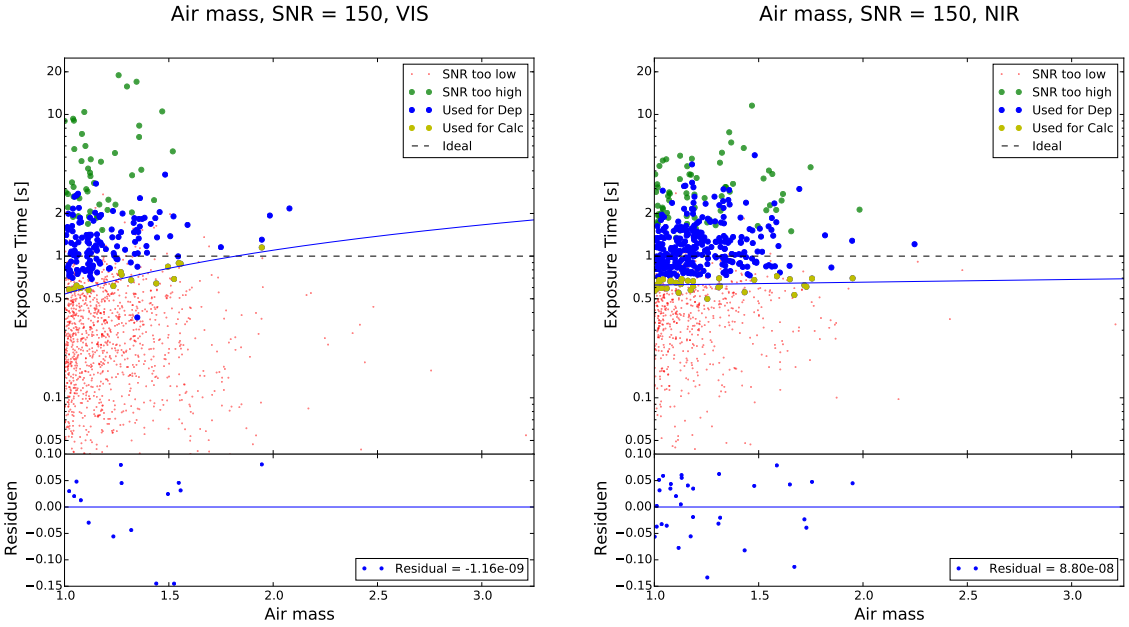

Figure 4.4: Top: Norm. time vs airmass, lower envelope fit (blue line) with feasible data (yellow points), observations within $SNR = 150 \pm 20\%$ (blue points), observations above $SNR = 150 + 20\%$ (green points), observations below $SNR = 150 - 10\%$ (red points) Bottom: residuals of the lower envelope fit

The extinction coefficients of Mauna Kea mentioned in Ch. 3.4 showed a 10 times higher extinction (loss of J/airmass) for the Vis than for the NIR and would lead to a difference of 0.17 mag for 2 air mass. In the end our ratio between the dependency of VIS and NIR was around 18. We would increase the exposure time in the VIS by over 50% while the calculation via Eq. 2.1 would suggest around 12% for a loss of 0.2 mag with air mass 2. For the NIR we increase the time by 3% while calculate 1,7% for a loss of 0.03 mag. Again these extinction values were for Mauna Kea while I did not find them for Calar Alto but i do not expect them to be as high as they needed to be to get to an increase of 50% on the exposure time. So this must be looked at again because the lower points at 1.5 air mass can might also suggest a smaller dependency.

4.4 Weather

By the first look at the plots for the weather (see Fig. 4.5) it was not easy to decide how to evaluate the dependency. Therefore many methods for the selection of the used points (blue points) were tried. We could not just stick to the lower points because for partly cloudy weather this could maybe mean the observations were not affected by the clouds at all. But also using every point could mean looking at unwanted effects, that hide in the upper extreme values for each weather type like the chemtrails or spiderwebs for "clear".
So in the end we threw away 5% of the extreme values and looked at the median (magenta points) for each weather type and took the relation to the photometric type as the dependency for the exposure time. The relation to the photometric type was chosen because in the visual wavelengths practically nothing disturbs the view in the sky. But the percentage range might need to be changed for future calculations because of the amount of times a partly cloudy observation is not affected by the clouds.
Because of the sheer mass of clear observations and the uncertainties of what was called "mostly clear" and "partly cloudy" that did not affect the observation we have a big increase in the dependency from photometric to clear and then only a small increase in the dependency for cirri and in the NIR even for clouds.

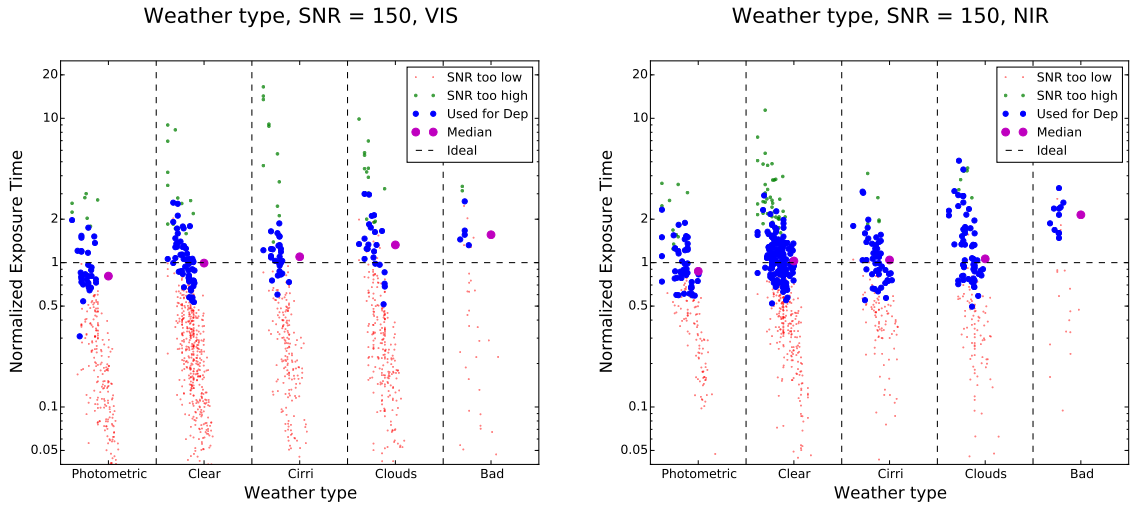

Figure 4.5: Norm. time vs weather types split up with the J band magnitudes (4 mag on the left to 12 mag on the right) in the respective weather type, median of data without the 5% extreme points (magenta points), observations within $SNR = 150 \pm 20\%$ (blue points), observations above $SNR = 150 + 20\%$ (green points), observations below $SNR = 150 - 10\%$ (red points)

Table 4.4: The different weather correction factors (c_{air}) for VIS and NIR

Condition	Vis	δVIS	NIR	δNIR
c_{Photo}	1	0.127	1	0.261
c_{Clear}	1.231	0.364	1.179	0.418
c_{Cirri}	1.361	0.340	1.197	0.487
c_{Cloud}	1.645	0.499	1.219	0.510
c_{Bad}	1.934	0.335	2.459	0.905

4.5 Extinction

As previous suspected in Ch. 3.6 the Extinction plot Fig. 4.6 had too few points in a relevant lower envelope area to even try any kind of dependency analysis and so we have to wait for more observations. It could still be the case that a high amount of the dependency for the extinction is already included in the air mass and weather type dependency and the extinction will not provide more information for our exposure time and so this needs to be checked later again.

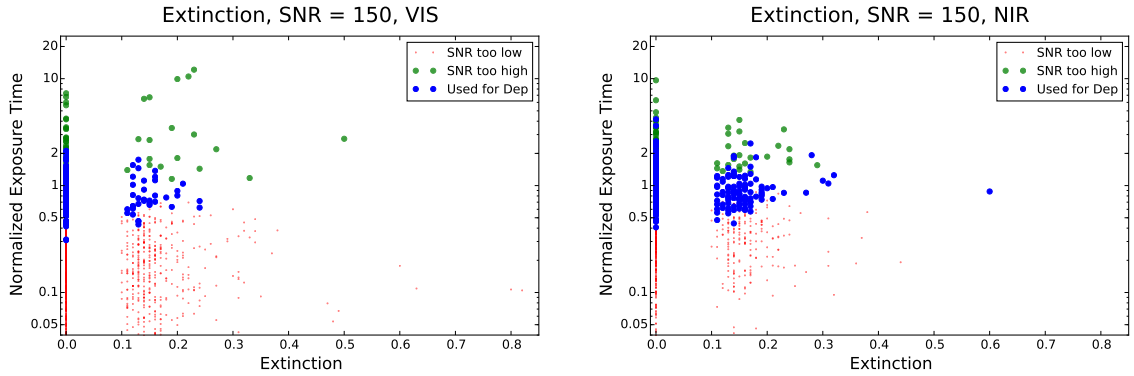

Figure 4.6: Norm. time vs extinction, observations within $SNR = 150 \pm 20\%$ (blue points), observations above $SNR = 150 + 20\%$ (green points), observations below $SNR = 150 - 10\%$ (red points)

4.6 Spectraltype

The same goes for the spectral type. We took a look at Fig. 3.4 earlier and wanted to check out if we still see a dependency for earlier and later spectral types. But by the look of Fig. 4.7 we have two horizontal lower boundaries in the area of M0 - M2 for the VIS and M0 - M4 in the NIR where sufficient points (blue points) are provided but the interesting relation we were looking for should come with the later types (>M4) and so we decided not to include the SpT into our exposure time calculations.

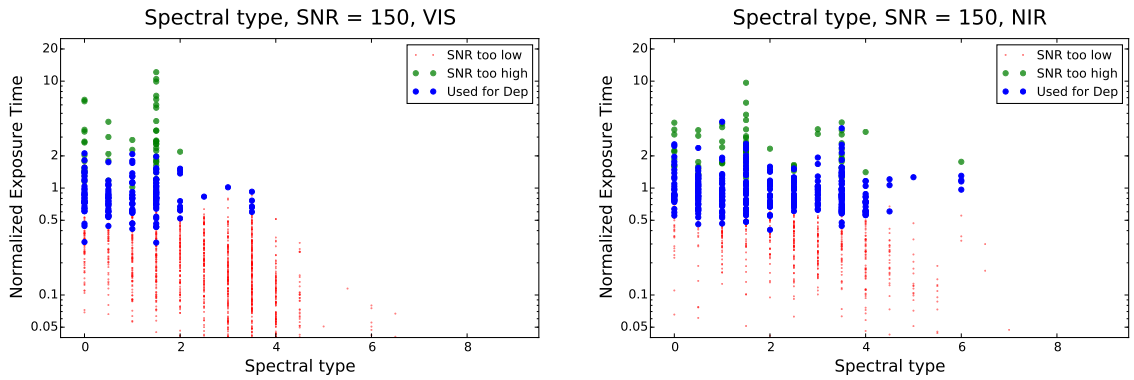

Figure 4.7: Norm. time vs SpT, observations within $SNR = 150 \pm 20\%$ (blue points), observations above $SNR = 150 + 20\%$ (green points), observations below $SNR = 150 - 10\%$ (red points)

4.7 Other Parameters

So at last we take a short look at a few other parameters in Fig. 4.8 for the VIS and Fig. 4.9 for the NIR. Given the problems we already had with the other corrections we can only search for very obvious outliers and then recommend later checking.
In the top left we see that for wind speed up to $10m/s$ we have sufficient datapoints and the lowest points build nearly a horizontal line but for higher speeds there seems to be an increase which should be looked at again.
To the right side we have the wind direction. Here the only eye catcher were the very few observations with a wind direction from around 95° up to 145°. Either some local wind streams cause this effect or the monitoring device needs to be checked.
In the bottom on the left we have the temperature. For the extreme degrees we miss the latest observations with more of the hot summer nights and the beginning of a full winter cycle so again its hard to give a definite answer but the NIR suggests that there might be a slight correction for the higher temperatures but it would still be nice to have a temperature gradient during the observation although it will not be correctable.
In the middle is the relative humidity. Here we need definitely more data for the VIS, because the air mass extinction depends also on the water vapor and it might be that there is a small slope in the lower boundary.
And at last on the right the pressure which only shows a few outliers around $785hPa$. Again there could be an error with the monitor or some abnormal chance with the observations.

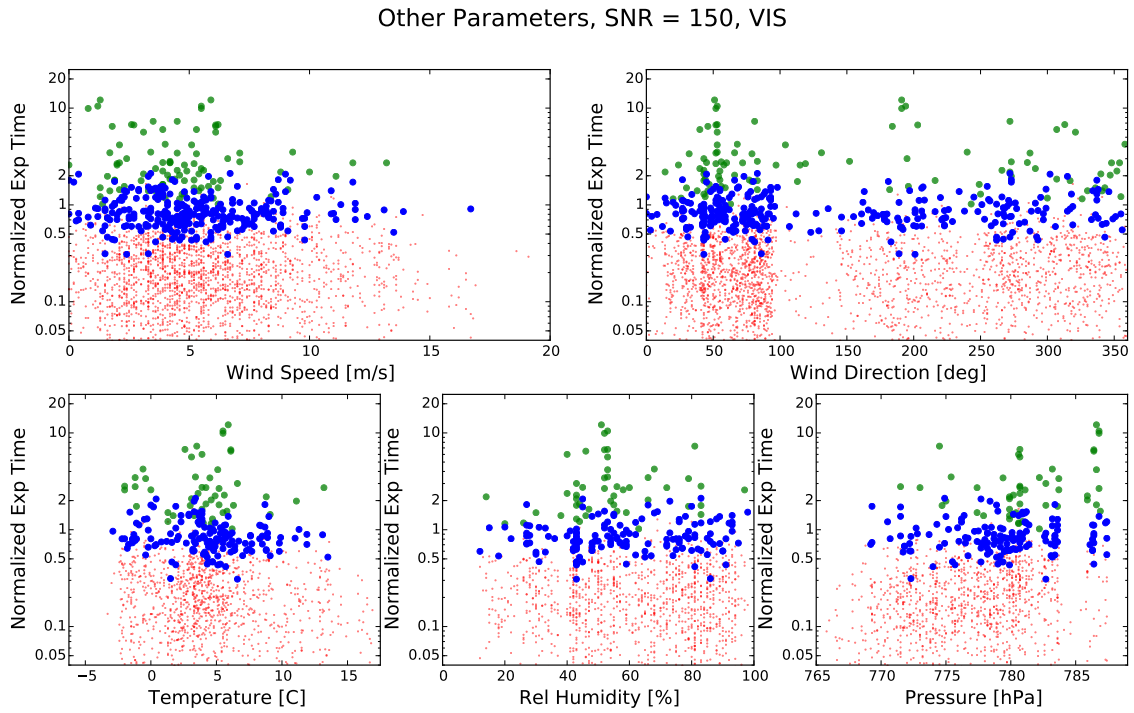

Figure 4.8: Other parameters plotted along with the visual data:
Top: wind parameters (left: speed, right; direction)
Bottom: left: temperatur, center: rel. humidity, right: pressure
observations within $SNR = 150 \pm 20\%$ (blue points), observations above $SNR = 150 + 20\%$ (green points), observations below $SNR = 150 - 10\%$ (red points)

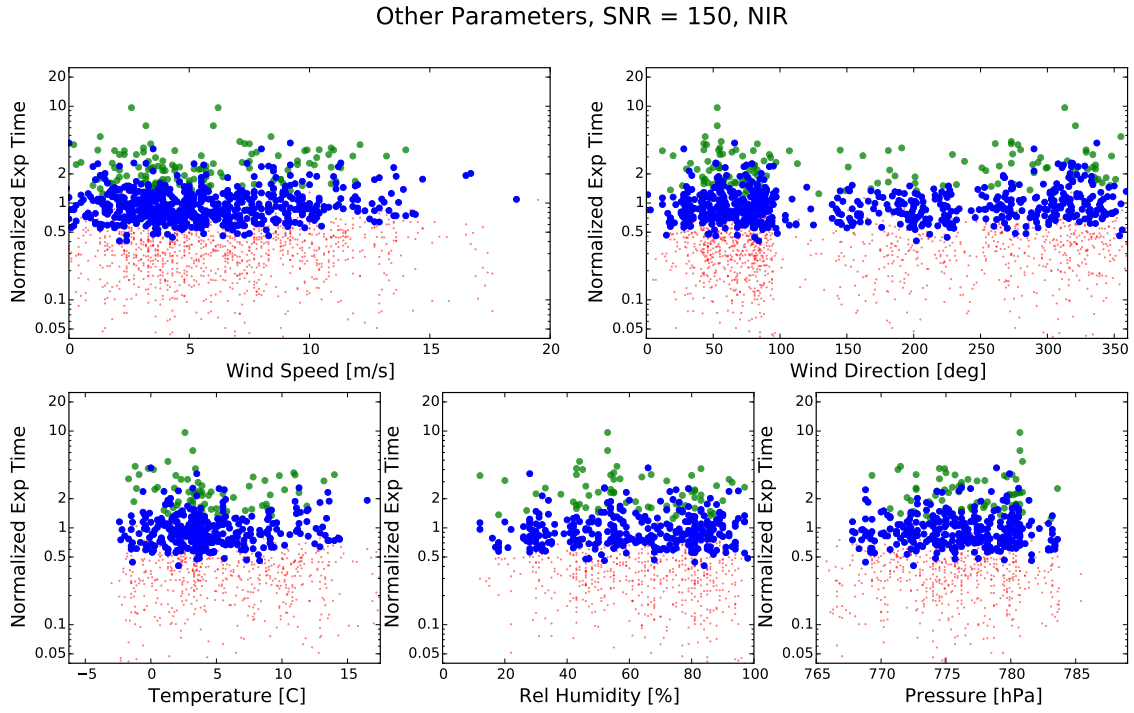

Figure 4.9: Other parameters plotted along with the near infrared data:
Top: wind parameters (left: speed, right; direction)
Bottom: left: temperatur, center: rel. humidity, right: pressure
observations within $SNR = 150 \pm 20\%$ (blue points), observations above $SNR = 150 + 20\%$ (green points), observations below $SNR = 150 - 10\%$ (red points)

5 The results

5.1 The precision of the calculations

At first we take a look at the result in dependency of the observation date to make sure we have no systematic error based on changes at the telescope, the pipeline or something else. But there does not seem to be any kind of problem like that and all the important points (blue for 20% range, magenta for 10%) seem to be in a more (NIR) or bit less(VIS) normal distribution around 1 or a bit below. For the VIS (Fig. 5.1) it might be possible to assign a normalized data point to the correct median SNR, which would be a another indication of a good calculation.

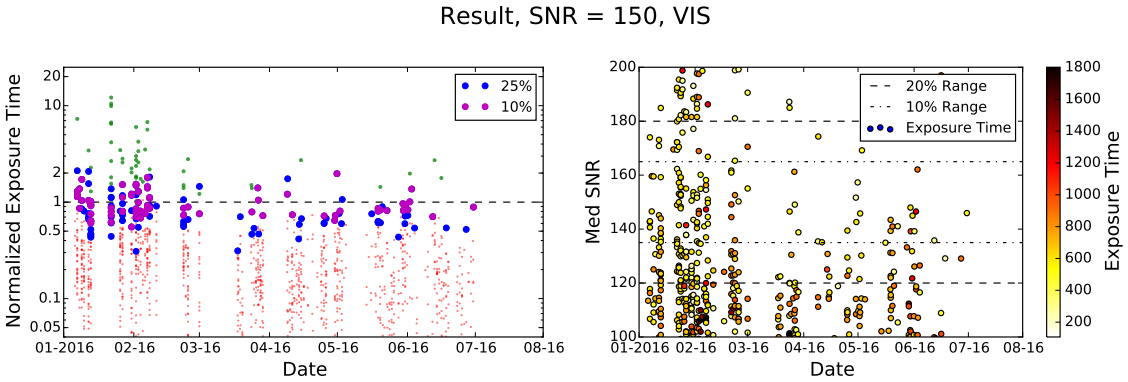

Figure 5.1: Visual result
Left: Observation date based result, observations within $SNR = 150 \pm 20\%$ (blue points), observations within $SNR = 150 \pm 10\%$ (magenta points), observations above $SNR = 150 + 20\%$ (green points), observations below $SNR = 150 - 10\%$ (red points)
Right: Observation date based median with exposure time color coding

For the NIR this is not possible because of the greater amount of points and in the beginning of February the NIR shows some observations with way too long exposure times (see Fig. 5.2). This is due to some very unfriendly observation conditions which made it only possible to observe the brightest targets with normally way too long exposure times.
If we compare both from March ongoing when both channels recorded simultaneously the NIR has more overexposed (green points) observation due to the higher flux and also the underexposed (red points) observations all seem to need less extra time.
So now we can take a closer look at the VIS result in form of the histogram Fig. 5.3. At the top we only see the median SNR of 150 and values in the 20% (blue bars) and 10% (green bars) area around them. The median for both is slightly below 1 which

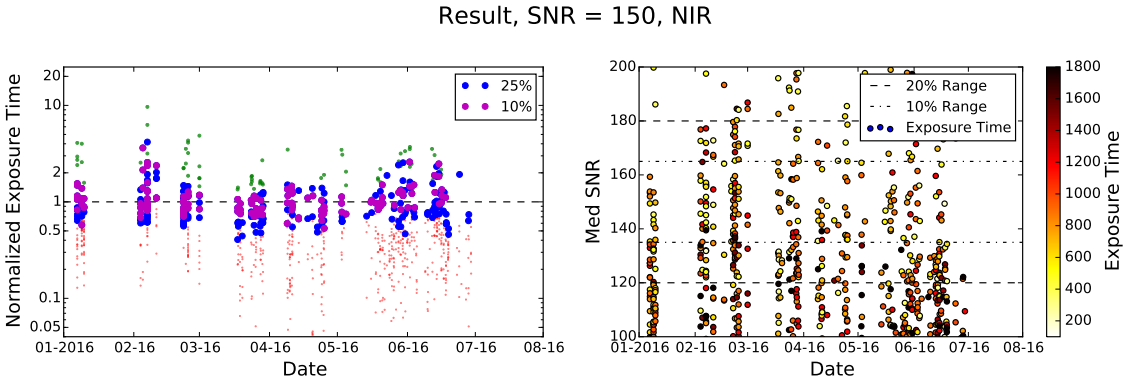

Figure 5.2: Near infrared result
Left: Observation date based result, observations within $SNR = 150 \pm 20\%$ (blue points), observations within $SNR = 150 \pm 10\%$ (magenta points), observations above $SNR = 150 + 20\%$ (green points), observations below $SNR = 150 - 10\%$ (red points)
Right: Observation date based median with exposure time color coding

means we needed more exposure time in general for the analyzed observations but that is not surprising because if we take a look at Fig. 5.1 again also more of the medians fall below 150 than above. Additionally a standard deviation of around 0.2 makes this an overall very satisfying calculation given that the seeing and weather dependencies caused big problems. The bottom of Fig. 5.3 (and later also for the NIR in Fig. 5.4) shows us additionally how all the other SNR ranges fall in relation to 150 and again how the ranges contribute to the precision of the calculation with the SNR $<$ 150 (yellow bars) peak below 1 and the SNR $>$ 150 (black bars) with less observations with more of a plateau from 0.9 to 2 instead of a peak.
Now for the NIR Fig. 5.2 showed us a more evenly distributed median SNR over the 10% (magenta Points) and 20% (blue points) range so we already expect a better calculation and Fig. 5.4 supports that with medians of nearly 1. But because of the already mentioned bad nights in February the distribution has a tail to some higher normalized times causing a slight increase in the standard deviation compared to the VIS. At this point we again have to keep in mind that we still do not know if SNR 150 really relates to $\delta RV = 1m/s$ and take this as a preliminary result for the exposure time calculator until the correct SNR is known. Again the lower plot shows the peak for the lower SNR (yellow bars) below 1 but this time with more observations above 1 and for the higher SNR (black bars) a peak around 1.2 instead of the plateau.
So at last we compare the time calculations in the I band from Ignasi Ribas(web [g]) with a few different calculations of my ETC. His equation was :

$$t(J) = 40 \times 10^{(J-4.2)/2.5} \tag{5.1}$$

We have to keep in mind that the lowest points are based on observations with way too long exposure times and the higest points with very low SNR due to the

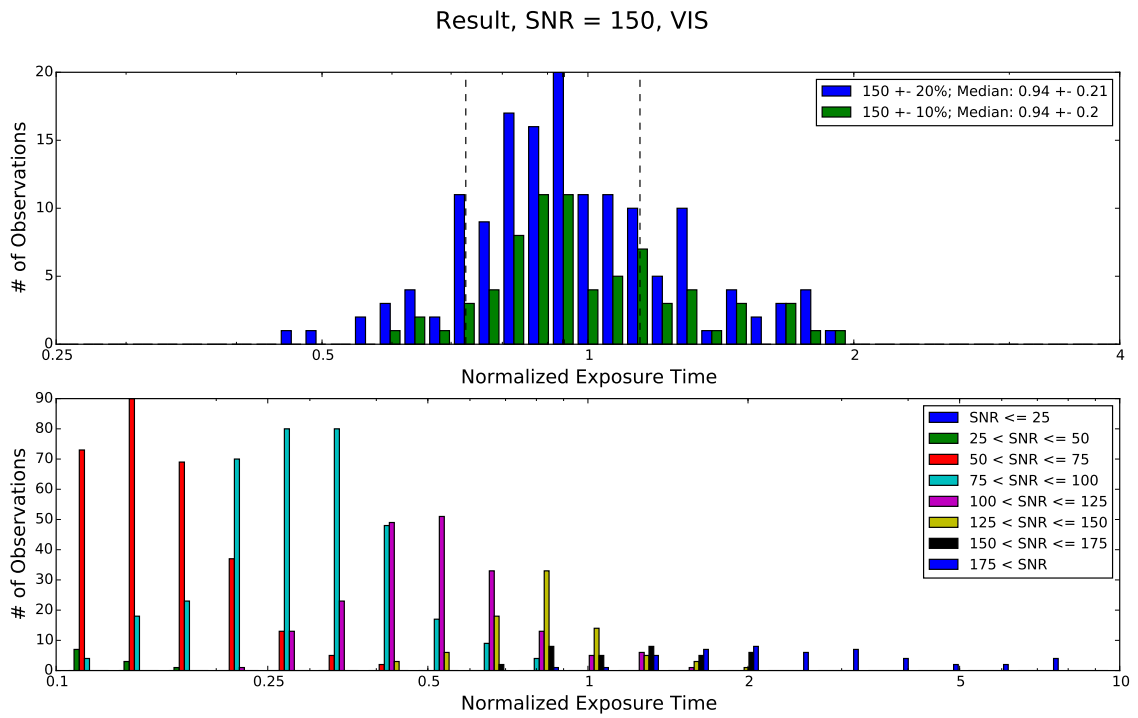

Figure 5.3: Visual result; Top: Norm. time histogram for 2 errors around SNR 150, observations within $SNR = 150 \pm 20\%$ (blue bars), observations within $SNR = 150 \pm 10\%$ (green bars), 20% σ with dashed lines,
Bottom: Histogram of different SNR ranges and the normalized time, most important: observations within $125 < SNR < 150$ (yellow bars), observations within $150 < SNR < 175$ (black bars)

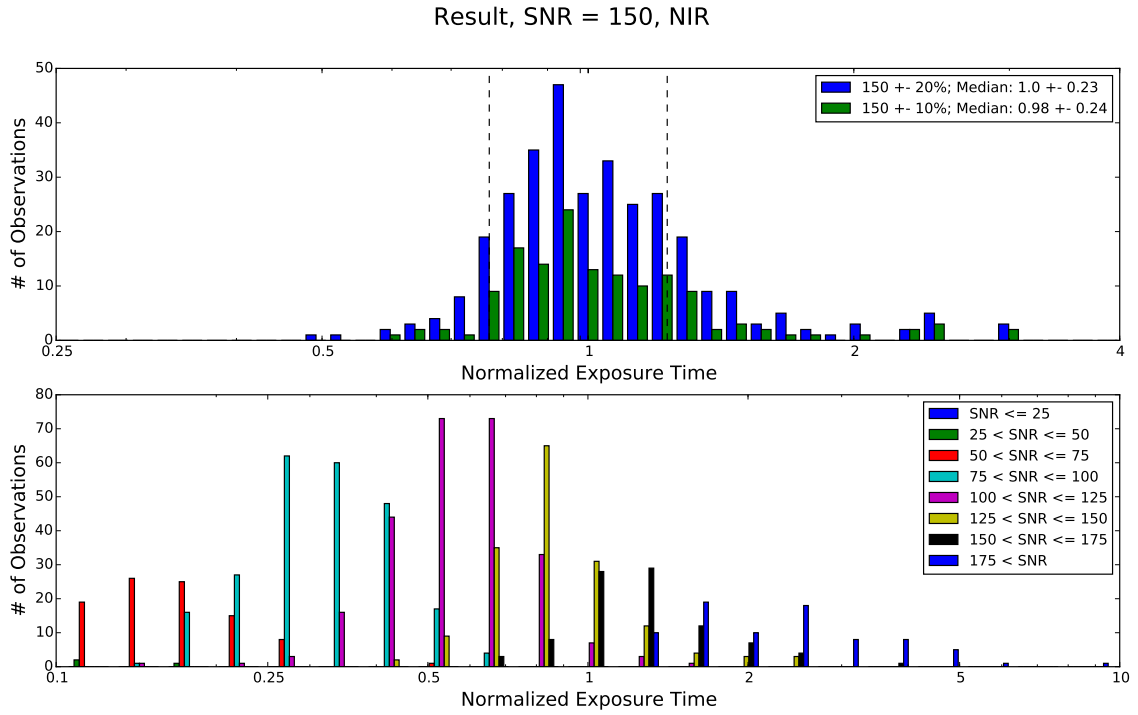

Figure 5.4: Near infrared result; Top: Norm. time histogram for 2 errors around SNR 150, observations within $SNR = 150 \pm 20\%$ (blue bars), observations within $SNR = 150 \pm 10\%$ (green bars), 20% σ with dashed lines,
Bottom: Histogram of different SNR ranges and the normalized time, most important: observations within $125 < SNR < 150$ (yellow bars), observations within $150 < SNR < 175$ (black bars)

conditions or other problems. Therefore the recalculation to SNR 150 is an estimation by Eq. 2.1 and of course not accurate.

First of all because I has less flux and based on only one extreme order Ribas's calculations are too low for the median over nearly the whole VIS channel. Additionally his calculations do not include any kind of observation conditions and dependencies and are therefore only a rough minimal estimate which is by the look of Fig. 5.5 way too low for the brightest stars and might just cover the needed exposure time when we get above 7.75 mag and 1000s and reach the max exposure time of 1800s by 8.33 mag.

Unsurprisingly this means it is not really usable with the median and we can take a look at my calculations which are based on the settings in Tab. 5.1, cover a wide range of observations and can be changed to every needed condition.

Table 5.1: Settings for the different conditions

Condition	Seeing	Airmass	Weather
Best conditions	1	1.15	Photo
Bad seeing	3	1.15	Photo
Bad air mass	1	2	Photo
Bad weather	1	1.15	Clouds
Bad conditions	3	2	Clouds

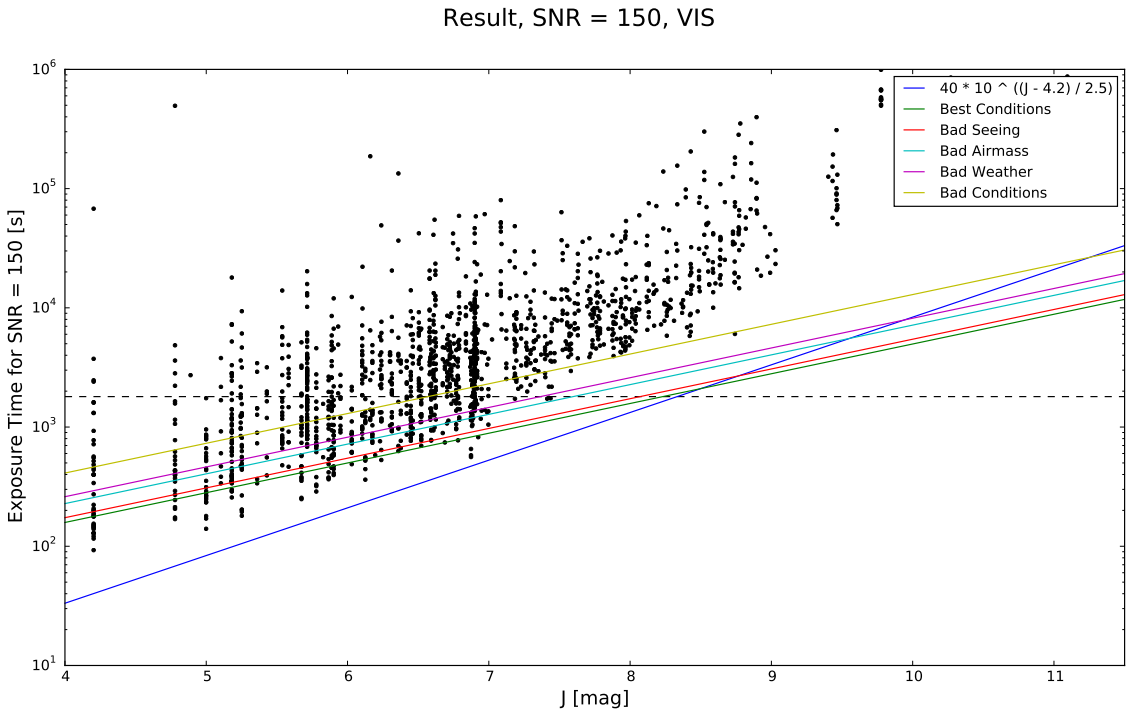

Figure 5.5: Visual result with all times calculated to SNR 150 with Eq. 2.1
comparison of different fits including Ignasi Ribas fit (blue) from the Redmine Wiki (web [g]), all best conditions fit (green), best conditions with bad seeing fit (red), best conditions with bad air mass fit (cyan), best conditions with bad weather type fit (magenta), worst conditions fit (yellow), settings and values are shown in Tab. 5.1

The same goes for the NIR (see Fig. 5.6). Now Ribas's calculations are not even based on the same detector anymore and should not even be considered especially with the not known relation of the SNR to δRV. This time my calculation for different conditions do not seem to cover that much observations because of the compared to the VIS low impact of the higher air mass and weather dependency. Many points are below my calculations because the VIS limits the observations and the SNR gets higher than needed so that the recalculation with Eq. 2.1 resulted in lower exposure times.

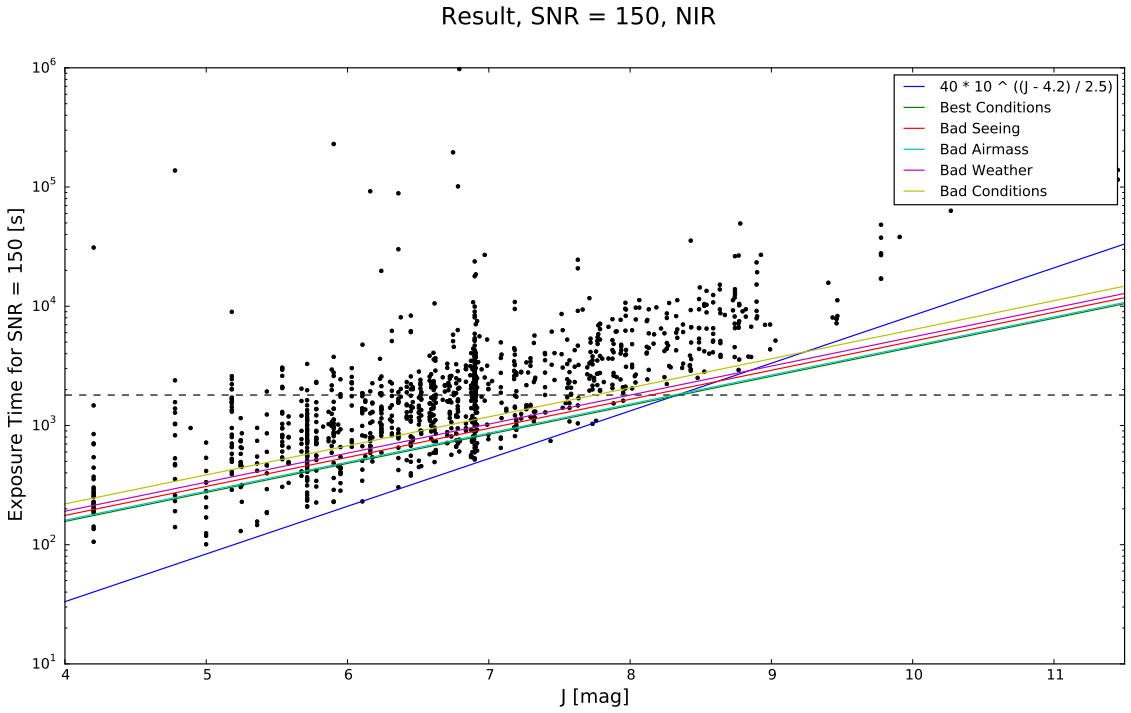

Figure 5.6: Near infrared result with all times calculated to SNR 150 with Eq. 2.1
comparison of different fits including Ignasi Ribas fit (blue) from the Redmine Wiki (web [g]), all best conditions fit (green), best conditions with bad seeing fit (red), best conditions with bad air mass fit (cyan), best conditions with bad weather type fit (magenta), worst conditions fit (yellow), settings and values are shown in Tab. 5.3

5.2 Calculation errors and their propagation

We started with a relatively difficult fit for the connection of J with the SNR and exposure time and therefore got relatively high uncertainties on the coefficients shown in Tab. 5.2. Additionally we got errors of unknown dimensions for the seeing values from the nightlogs (sometimes around 1 arcsec) that a propagation of the uncertainties would have increased the errors into dimensions which would have made any other calculation obsolete. Hence we decided not to include the propagation of errors, but that can be revised at a later stage when more observations improve the $t(J)$ fit and maybe enough header files include seeing information which than can be handled by the calculator or the information in the nightlogs get improved.

Table 5.2: The correction factors with their respective absolut error

Condition	Vis	δVIS	NIR	δNIR
m_{J}	15.379	2.794	16.007	2.100
c_{J}	0.575	0.029	0.561	0.019
SNR_{med}	145.390	11.910	151.025	12.444
c_{see}	5.660E-3	1.188E-3	7.246E-3	0.809E-3
c_{air}	0.561	0.076	0.030	0.037
c_{Photo}	1	0.127	1	0.261
c_{Clear}	1.231	0.364	1.179	0.418
c_{Cirri}	1.361	0.340	1.197	0.487
c_{Cloud}	1.645	0.499	1.219	0.510
c_{Bad}	1.934	0.335	2.459	0.905

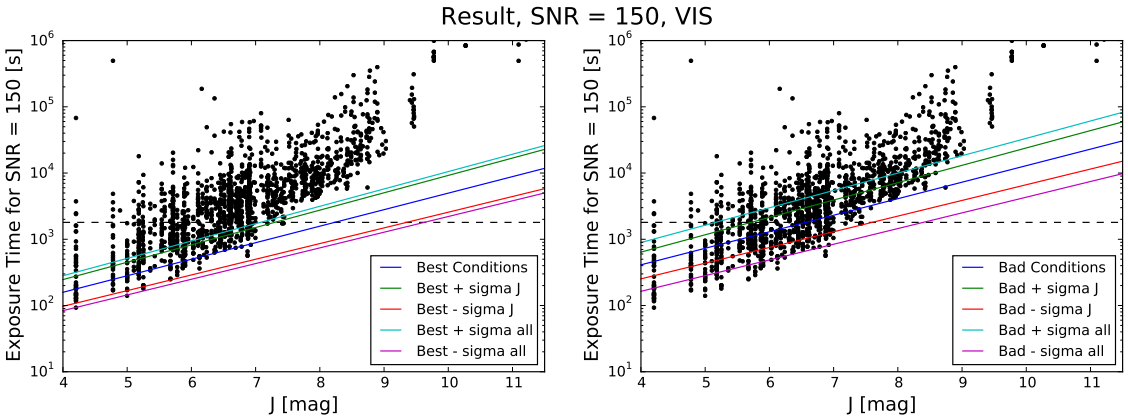

Figure 5.7: Visual uncertainties
Best (left) and worst (right) conditions (blue) and the corresponding error plots, $+\sigma_J$ in green, -σ_J in red, $+\sigma_{all}$ in cyan, -σ_{all} in magenta

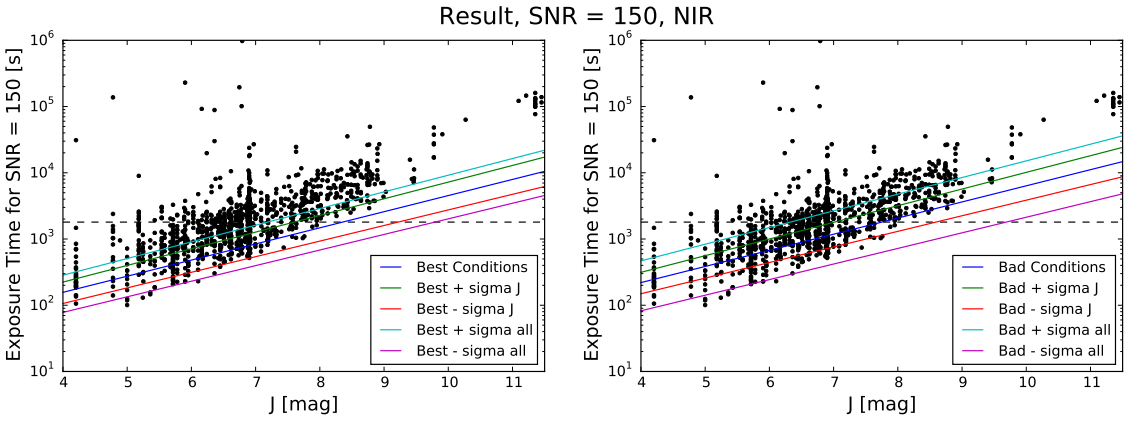

Figure 5.8: Near infrared uncertainties
Best (left) and worst (right) conditions (blue) and the corresponding error plots, $+\sigma_J$ in green, -σ_J in red, $+\sigma_{all}$ in cyan, -σ_{all} in magenta

The relative error for the NIR air mass correction got so huge because of the nearly horizontal linear fit and the errors for the the weather types are so large because of the great amount of data sets used for the median calculation and the error propagation to the ratio. Fig. 5.7 and Fig. 5.8 illustrate the big impact of the $t(J)$ fit for good and bad conditions and makes you wonder on the implications on the seeing uncertainties an then further on. So for now for the VIS the initial time calculation remains the source for the biggest error. While for the NIR the sum of the other conditions outweigh the time calculation error during the bad conditions.

5.3 The ETC

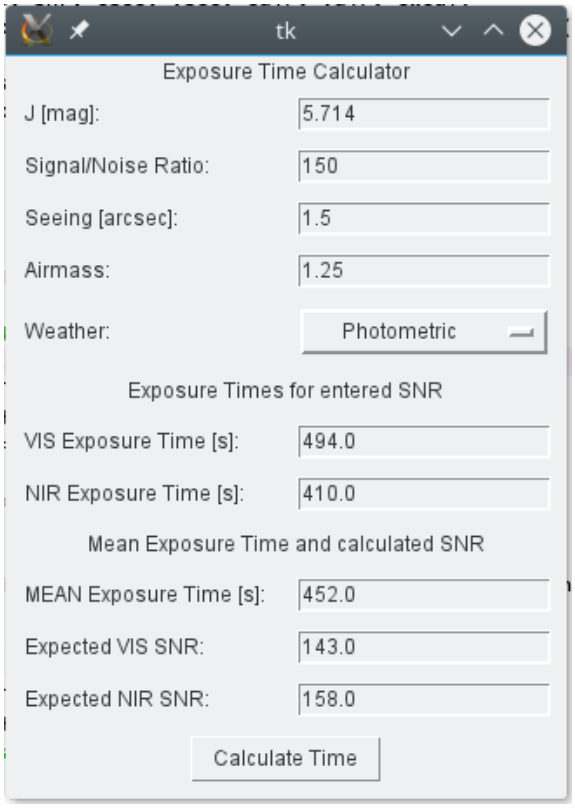

Figure 5.9: The programmed calculator GUI
In the top half are the input fields for J, SNR, seeing and airmass and a drop down menu for the weathertypes
In the bottom half are the exposure time calculations and for the mean time a calculation of the SNR with Eq. 2.1

In the end my programmed ETC is just a simple GUI with the input of J, SNR, seeing, air mass and a drop down menu to select the weather type. The general equation for the calculation is:

$$t_{exp} = m_{\mathrm{J}} e^{c_{\mathrm{J}} \times J} \times (1 + c_{see} e^{see}) \times (1 + c_{air}(air - 1)) \times c_{\mathrm{wt}} \times \left(\frac{SNR}{SNR_{\mathrm{med}}} \right)^2 \quad (5.2)$$

The coefficients can be taken from Tab. 5.2 with SNR_{med} from the $t(J)$-fit. Addi-

tionally we get an output of the mean exposure time and with Eq. 2.1 an estimation for the SNR gets calculated.
The calculator is fully standalone because the coefficients for SNR 150 are programmed into it but via EQ. 2.1 the exposure times for any desired SNR can be calculated. When a suitable connection for δRV to the SNR is found for the NIR this should be changed maybe even to an input of δRV.
At last in Tab. 5.3 are some example calculations for 4 stars with 5 different observations conditions also shown in Fig. 5.5 and Fig. 5.6.

Table 5.3: A few example values from the ETC for SNR 150

Star	J band	Seeing	Airmass	Weather	VIS time	NIR time	Mean
Lalande	4.203	1	1.15	Photo	195	172	184
Luytens	5.714	1	1.15	Photo	465	401	433
Ross 905	6.9	1	1.15	Photo	920	780	850
GJ 643	7.555	1	1.15	Photo	1340	1126	1233
Lalande	4.203	3	1.15	Photo	214	193	204
Luytens	5.714	3	1.15	Photo	511	451	481
Ross 905	6.9	3	1.15	Photo	1009	876	943
GJ 643	7.555	3	1.15	Photo	1470	1265	1368
Lalande	4.203	1	2	Photo	281	176	229
Luytens	5.714	1	2	Photo	670	411	541
Ross 905	6.9	1	2	Photo	1325	800	1062
GJ 643	7.555	1	2	Photo	1800	1154	1477
Lalande	4.203	1	1.15	Clouds	321	210	265
Luytens	5.714	1	1.15	Clouds	766	489	627
Ross 905	6.9	1	1.15	Clouds	1513	951	1232
GJ 643	7.555	1	1.15	Clouds	1800	1373	1586
Lalande	4.203	3	2	Clouds	508	241	374
Luytens	5.714	3	2	Clouds	1209	563	886
Ross 905	6.9	3	2	Clouds	1800	1095	1447
GJ 643	7.555	3	2	Clouds	1800	1581	1690

6 Conclusion

Despite all the problems the ETC should be of great help for future observations. First of all it can give an output for every wanted magnitude and is not a table anymore like the one included in the manual which suggests a fixed time for a range of magnitudes. It will also be better than Ignasi Ribas's calculations which were only based on the maximum SNR order and not useful over a wide range of orders which is needed for precise radial velocity evaluations. Furthermore it includes minimum adjustments for different observation conditions helping the observer to adjust the time based on actual data. Based on this calculations they then can include their own corrections based on their experience if they seem fitting for the night.
But if we look at the uncertainties and problems again at this stage the calculator of course is not the perfect solution but a nice guideline. The initial exposure time calculations should be remade from time to time with a greater set of samples and then the range of included data can be minimized for further optimization or the data can be presorted for great observation conditions. The fitted dependence on the seeing must be improved by either waiting for enough data from the header files and then using that data or by enforcing more and better descriptions in the night-logs. Most suitable would be notes to every observation. The weather logs should include more timestamps so that the changes in weather can be allocated to the right observations later. And again it would be best to have a separate information for each observation. More observations with extinction values are needed to check if there is another dependency or if this is covered by the air mass and weather.
After this is done the recalculation of the air mass dependency should not be a problem given that the points for air mass > 1.5 are available and then we can start to take a closer look at the other parameters which I only briefly mentioned. Furthermore it might be good to include information of the moon brightness and direction compared to the telescope to determine if and how much the influence on the SNR might be.
This means the calculator can be made publicly available on the website of CARMENES so everybody can calculate their SNR and exposure times for their project. Furthermore the ETC could be sent to Calar Alto to maybe include it directly in to the Instrument Control System for direct access during the night. But it should be updated from time to time to ensure and improve the quality of the calculations and be mentioned how accurate the dependencies are.

7 Bibliography

Exoplanet Encyclopaedia, a. URL http://exoplanet.eu/.

Gemini air mass extinction, b. URL https://www.gemini.edu/sciops/telescopes-and-sites/observing-condition-constraints/extinction.

K2-33 Newborn Exoplanet, c. URL http://www.jpl.nasa.gov/news/news.php?feature=6539.

Alpha star list, d. URL https://carmenes.caha.es/int/gto/alpha.txt.

Carmenes GTO archive, e. URL http://carmenes.cab.inta-csic.es/gto/.

Doppler effect drawing, f. URL http://web.mit.edu/knazemi/www/intermediateExperiment1.htm.

Redmine Issue 2393: ETC, g. URL https://redmine.ice.csic.es/issues/2393.

NIR echelle spectra, h. URL https://carmenes.caha.es/ext/instrument/DeltaLambdaNIR.txt.

Redmine Wiki, i. URL http://redmine.ice.csic.es.

Seeing example, j. URL http://www.noao.edu/education/gsmt/seeing.

Brinkmöller observation table, k. URL https://docs.google.com/spreadsheets/d/11b7UhYuIGFz0PWZyoBVnf0nFU8_OQKlzwJqcnBdl-hs/edit?pref=2&pli=1#gid=0.

M. Brinkmoeller. Analysis of the activity of M dwarfs observed by CARMENES assessed on the calcium infrared triplet, 2016.

K. Clubb. a detailed derivation of The Radial Velocity Equation, 2008.

A. Cumming, G.W. Marcy, and P. Butler. The Lick Planet Search: Detectability and Mass Thresholds. *The Astrophysical Journal, 526, 890-915*, 1999.

M. Kim. Preparation of the CARMENES target list, 2015.

D.W. Latham, T. Mazeh, R.P. Stefanik, M. Mayor, and G. Burki. The unseen companion of HD114762: a probable brown dwarf. *Nature, 339, 38-40*, 1989.

N. Reid and S. Hawley. *New Light on Dark Stars*. Springer Praxis Books, 2005.

S.F. Sanchez, U. Thiele, J. Aceituno, D. Perez-Ramirez, and J. Alves. The Night-Sky at the Calar Alto Obervatory. *Astronomical Society of Pacific, 119, 873, 1244-1254*, 2007.

S.F. Sanchez, U. Thiele, J. Aceituno, D. Cristobal, J. Perea, and J. Alves. The Night-Sky at the Calar Alto Obervatory II: The sky at the near infrared. *Astronomical Society of Pacific, 120, 860, 1186-1200*, 2008.

M. Zechmeister. *CARACAL: pipeline manual*, 1.02 edition, 2015.

M. Zechmeister, G. Anglada-Escudé, and A Reiners. Flat-relative optimal extraction. *Astronomy & Astrophysics, 561, A59*, 2014.

Erklärung

Ich versichere, dass ich diese Arbeit selbstständig verfasst und keine anderen als die angegebenen Quellen und Hilfsmittel benutzt habe.

Heidelberg, 15.09.2016 .....

Stefan Grohnert